On the Correspondence Between Output Limiting Backstepping and Higher-Order Control Barrier Functions

Agnes Steinert[1*], Hangxu Li[1] and Johannes Autenrieb[2]

[1*]Institute of Flight System Dynamics, Technical University of Munich, Boltzmannstr., Garching, 85748, stateBavaria, Germany.
[2]Department of Flight Dynamics and Simulation, Institute of Flight Systems, DLR (German Aerospace Center), Braunschweig, Germany.

*Corresponding author(s). E-mail(s): agnes.steinert@tum.de;
Contributing authors: hangxu.li@tum.de; Johannes.Autenrieb@dlr.de;

Abstract

Output Limiting Backstepping (OLB) and Higher-Order Control Barrier Functions (HOCBFs) both protect constrained system outputs through recursive constructions. This paper investigates their mathematical relationship and identifies conditions under which they yield identical limiting control inputs. The OLB formulation considered here requires a strict-feedback structure, whereas HOCBFs apply to a broader class of systems. For systems admitting both methods, the analysis shows how the HOCBF recursion corresponds to OLB phase-plane boundaries and tracking errors. It further establishes how to choose the safety function and design gains so that both methods yield identical limiting control inputs for relative degrees two and three. Aircraft angle-of-attack protection simulations confirm the correspondence and show that neglecting actuator dynamics can cause oscillations or instability under aggressive protection settings. The resulting correspondence provides a physical interpretation of HOCBF design parameters through OLB phase-plane limits and can guide HOCBF design for systems to which both methods apply.

Keywords: Control barrier functions, Safety filters, Output limiting, Output limiting backstepping, Flight envelope protection

1 Introduction and Motivation

Control Barrier Functions (CBFs) are a method for keeping dynamical systems within predefined safety limits, such as maximum velocities, minimum distances, or operating boundaries. Early research by Prajna and Jadbabaie introduced barrier certificates, which provide a mathematical way to verify whether a system will remain within its safe operating region Prajna and Jadbabaie (2004). Wieland and Allgöwer subsequently introduced CBFs as a means of designing controllers that actively prevent violations of safety constraints Wieland and Allgöwer (2007). Ames and coauthors further developed this concept into optimization-based safety filters that modify the commands of an existing controller only when necessary to maintain safety Ames et al. (2014, 2017a). However, conventional CBF formulations are not directly applicable when the protected output has a relative degree higher than one, meaning that the control input influences the output only through higher-order derivatives. To address this limitation, Nguyen and Sreenath introduced Exponential Control Barrier Functions Nguyen and Sreenath (2016), followed by the more general Higher-Order Control Barrier Function (HOCBF) formulation of Xiao and Belta Xiao and Belta (2022).

CBFs and HOCBFs have been applied in several fields, including robotics (Wang et al. 2024; Xiong et al. 2026; Heshmati-Alamdari et al. 2024), automotive systems (Sabouni et al. 2024; Ahmad et al. 2025), and energy systems (Feng et al. 2024; Schneeberger et al. 2024). Applications include collision avoidance in multi-agent systems (Bhatia et al. 2026), enforcing safety under actuator constraints (Rabiee and Hoagg 2025), and handling uncertain system dynamics (Gutierrez and Hoagg 2025). CBF-based methods are also used for safe human–robot interaction, including collision prevention and contact-force limitation (Vinter-Hviid et al. 2024; Liu et al. 2024; Sharma et al. 2025; Maithani et al. 2026), as well as maintaining safe operating conditions in industrial processes and power systems (Wang et al. 2025; Qin et al. 2026). In aerospace, CBFs have been applied to flight-envelope protection, including limits on angle of attack, load factor, and angular rates (Altunkaya et al. 2026; Autenrieb 2025).

CBF-based safety filters can be integrated at different levels of a control architecture. The intervention level determines which signal is modified to enforce safety constraints. Three approaches can be distinguished:

- **Control-input-level filtering:** The most common approach is to modify the control input generated by a nominal controller, often through a quadratic program, based on the plant dynamics (Hsu et al. 2024; Autenrieb et al. 2026). However, modifying the input to the plant that is generated by the nominal controller can change the nominal closed-loop response and may affect stability and robustness properties (Tan and Dimarogonas 2024; Autenrieb et al. 2026). Additional measures may be required to prevent, for example, controller integrators from winding up or reference models from drifting away in case the input is adjusted and, consequently, the commanded reference is not reached.

- **Pseudo-control-level filtering:** In many control architectures, like dynamic inversion for example, the safety filter can modify a virtual control signal, such as desired accelerations or generalized forces and moments, before its conversion into physical actuator commands (Govoni and Cristofaro 2024; Hafner et al. 2026). This can reduce the optimization dimension in overactuated systems and allows an existing control allocator to be retained. However, constraint satisfaction depends on whether the lower-level controller and allocator can realize the required pseudo-control. Also here additional wind-up strategies in the reference model or controller might be necessary.
- **Reference-command-level filtering:** Alternatively, the reference command can be modified before it enters the nominal controller. Barrier-function-based reference governors (Li and Atanasov 2023; Liang et al. 2024) and closed-loop-model-based CBF filters (Autenrieb et al. 2026) demonstrate this approach. Since the safety filter acts before the nominal controller, this avoids integrator windup or reference-model drfift caused by overriding the controller output. However, the safety-filter design must account for the closed-loop response, including the controller. This may be difficult to obtain for complex control architectures. Furthermore, changes to the nominal controller or its parameters may require corresponding updates to the closed-loop model used by the safety filter.

Flight-envelope protections have a long history in classical flight control, and besides the novel CBF-based safety filters, various approaches have been developed to enforce aerodynamic and structural limits. Particularly interesting are the phase-plane-based protection methods, which were developed and incorporated into physically integrated reference-model architectures in flight control (Zhang et al. 2013, 2014; Zhang and Holzapfel 2015). Phase-plane-based protections define admissible output rates as a function of the distance to a physical limit, thereby allowing the desired limiting behavior to be specified directly in physically interpretable quantities.

Building on this concept,. Steffensen et al. (2019a) introduced Output Limiting Backstepping (OLB), which combines phase-plane-based output-rate limits with a recursive backstepping design to determine the corresponding limiting control input. The approach also allows nonlinear and piecewise-polynomial phase-plane boundaries to shape the response near the constraint. OLB-related protections have been integrated into different flight-control architectures and investigated in simulations, including incremental flight control, fly-by-wire reference models, and reinforcement-learning-based worst-case testing (Karlsson et al. 2016; Gabrys et al. 2019; Steffensen et al. 2022; Braun et al. 2022).

Although HOCBFs and OLB originate from different mathematical formulations, both approaches address the same fundamental problem of protecting constrained system outputs. Moreover, both methods employ recursive constructions to derive the corresponding safety conditions or limiting control laws. These similarities raise the question of whether HOCBFs and OLB represent fundamentally different protection mechanisms or whether they are mathematically related and, under certain conditions, may even yield identical protection laws. Understanding this relationship is of particular interest because it may allow design principles, properties, and advantages

of one approach to be transferred to or exploited within the other. This motivates a systematic analytical comparison of both methods to identify their mathematical relationships, similarities, differences, and the conditions under which their protection laws coincide.

This paper investigates the relationship between HOCBFs and OLB and examines whether the two approaches can provide the same protection behavior. The main contributions are:

1. **Applicability of both methods:** We compare the two approaches and show that HOCBFs can be applied to a broader range of systems, while OLB requires a more specific system structure.
2. **Relationship and equivalence:** We derive the mathematical relationship between HOCBFs and OLB and show that, for systems where both methods can be applied, their design parameters can be chosen such that they produce identical protection. We identify the conditions under which this equivalence holds.
3. **Transfer of design principles:** We show how the physically intuitive phase-plane limits used in OLB can be translated into the HOCBF formulation. This provides a way to design HOCBF protections based on the desired physical behavior rather than selecting design parameters based on simulations.
4. **Application to aircraft protection:** We demonstrate the results through simulations of aircraft angle-of-attack protection, both with and without actuator dynamics. The examples show that the two approaches can produce identical protection behavior and illustrate why accounting for actuator dynamics is important, particularly when designing less conservative protections.

The remainder of this paper is organized as follows. Section 2 introduces the common general output-protection problem. Sections 3 and 4 present the HOCBF and OLB approaches, respectively. Section 5 first compares both methods using a simple aircraft angle-of-attack protection example with one backstepping step to illustrate their mathematical relationship. Section 6 extends the analysis beyond this example and derives the general relationship between both methods, including the additional conditions required when more backstepping steps are involved. Section 7 then applies these results to the aircraft example with actuator dynamics, which require an additional backstepping step. The simulations demonstrate the derived correspondence and illustrate cases where it can make sense to account for actuator dynamics in the protection design. Finally, and 8 provides the conclusions.

2 Common Output-Protection Problem

Higher-order control barrier functions (HOCBFs) and output limiting backstepping (OLB) are derived based on different mathematical constructions. However, both methods can be used to address the same problem: protecting a constrained system output. Before introducing the two methods, this section defines the common output-protection problem.
Consider a nonlinear dynamical system with state $\boldsymbol{x} \in \mathbb{R}^n$ and a scalar protected

output

$$y = p(\boldsymbol{x}). \tag{1}$$

The output is subject to the upper physical limit

$$y \leq y_{\max}. \tag{2}$$

The corresponding safe output set is

$$\mathcal{Y}_{\text{safe}} = \{y \in \mathbb{R} \mid y \leq y_{\max}\}. \tag{3}$$

For clarity, the following derivations consider an upper output limit as given in Eq. (2). The corresponding formulations can analogously be established for a lower output limit. Restricting the presentation to the upper-limit case avoids repeated sign-dependent formulations and makes the subsequent derivations easier to follow.

Both methods, OLB and HOCBF, aim to leave the nominal control behavior unchanged unless a safety intervention is required. Protection becomes active when the nominal input command u generated by the controller would lead to a violation of the respective safety condition $y \leq y_{\max}$. However, though they share this common objective, the two methods differ in how the safety condition is formulated and how the corresponding safety-modified control input is obtained, as will be shown in the following sections.

3 Higher-Order Control Barrier Functions

Higher-order control barrier functions (HOCBF) extend the CBF concept to safety constraints for which the physical control input does not appear in the first derivative of the so-called safety function H. The formulation presented in this section builds on the CBF framework in Ames et al. (2017b) and the HOCBF construction for high-relative-degree constraints introduced in Xiao and Belta (2019), adapted here to the notation and output-protection problem considered in this paper. We first define the class of systems for which the HOCBF formulation considered in this paper can be applied. We then introduce the safety function H, explain how it represents the physical output constraint, and define the corresponding safe state set. Based on this representation, we determine the relative degree of H to identify after how many derivatives the physical control input appears. This motivates the recursive HOCBF construction. Finally, the forward-invariance result shows under which conditions the HOCBF construction guarantees satisfaction of the original output constraint and allows the resulting restriction on the physical control input to be derived.

3.1 Input-Affine System and Output-Based Safety Representation

The HOCBF formulation considered in this paper can be applied to controlled nonlinear input-affine systems of the form

$$\dot{\boldsymbol{x}} = \boldsymbol{f}(\boldsymbol{x}) + \boldsymbol{g}(\boldsymbol{x})\boldsymbol{u}, \qquad \boldsymbol{x} \in X \subseteq \mathbb{R}^n, \qquad \boldsymbol{u} \in \mathbb{R}^m, \tag{4}$$

with $\boldsymbol{f} : X \to \mathbb{R}^n$ and $\boldsymbol{g} : X \to \mathbb{R}^{n\times m}$.

The protected scalar output $y = p(\boldsymbol{x})$ is subject to the upper limit $y \leq y_{\max}$. To formulate this constraint as a CBF, it is represented by a continuously differentiable output-space safety function.

Definition 1 (Output-Space Safety Function) Let $h : \mathbb{R} \to \mathbb{R}$ be a continuously differentiable function selected such that

$$h(y) \geq 0 \quad \Longleftrightarrow \quad y \leq y_{\max}. \tag{5}$$

A simple choice can, for example, be $h(y) = y_{\max} - y$.

Since the protected output is determined by the system state, substituting $y = p(\boldsymbol{x})$ into the safety function in Eq. (5) gives

$$H(\boldsymbol{x}) := h(p(\boldsymbol{x}))\,, \qquad H(\boldsymbol{x}) \geq 0. \tag{6}$$

Definition 2 (Safe State Set) The corresponding safe state set is

$$\mathcal{X}_{\text{safe}} = \{\boldsymbol{x} \in X \mid H(\boldsymbol{x}) \geq 0\}\,. \tag{7}$$

Thus, $\mathcal{X}_{\text{safe}}$ contains exactly those system states for which the protected output satisfies $y \leq y_{\max}$. The HOCBF design must therefore ensure that the system remains in $\mathcal{X}_{\text{safe}}$. Whether the control input $\boldsymbol{u}$ can directly enforce this condition depends on the relative degree of $H(\boldsymbol{x})$, which is considered next.

3.2 Relative Degree of the Safety Function

The safety condition $H(\boldsymbol{x}) \geq 0$ can constrain the physical control input when $\boldsymbol{u}$ appears in a time derivative of H. The relative degree therefore determines how many derivatives of the safety function are required before the control input can directly affect the safety condition.

Differentiating $H(\boldsymbol{x}) = h(p(\boldsymbol{x}))$ from Eq. (6) and substituting the system dynamics from Eq. (4) gives

$$\begin{aligned}\dot{H} &= \frac{\partial H}{\partial \boldsymbol{x}}\left[\boldsymbol{f}(\boldsymbol{x}) + \boldsymbol{g}(\boldsymbol{x})\boldsymbol{u}\right] \\ &= \underbrace{\frac{\partial h}{\partial y}\frac{\partial p}{\partial \boldsymbol{x}}\boldsymbol{f}(\boldsymbol{x})}_{=:a_1(\boldsymbol{x})} + \underbrace{\frac{\partial h}{\partial y}\frac{\partial p}{\partial \boldsymbol{x}}\boldsymbol{g}(\boldsymbol{x})}_{=:b_1(\boldsymbol{x})}\boldsymbol{u}.\end{aligned} \tag{8}$$

If $b_1(\boldsymbol{x}) \neq 0$, the safety function has relative degree one. If $b_1(\boldsymbol{x}) = 0$, the physical control input does not appear in $\dot{H}$, and H must be differentiated again. Repeating this procedure gives

$$\begin{aligned}&H^{(1)} = a_1(\boldsymbol{x}), \quad H^{(2)} = a_2(\boldsymbol{x}), \quad \ldots, \quad H^{(r-1)} = a_{r-1}(\boldsymbol{x}), \\ &H^{(r)} = a_r(\boldsymbol{x}) + b_r(\boldsymbol{x})\boldsymbol{u}, \qquad b_r(\boldsymbol{x}) \neq 0.\end{aligned} \tag{9}$$

The same relations are commonly expressed using Lie derivatives in the CBF literature. For convenience the notation $a_i(\boldsymbol{x})$ and $b_i(\boldsymbol{x})$ is used here.

The safety function $H(\boldsymbol{x})$ has relative degree r if the physical control input first appears in its r-th time derivative. The relative degree depends on the output map $y = p(\boldsymbol{x})$, the safety function $h(y)$, and the system dynamics.

For $r > 1$, the safety condition must be extended recursively until the derivative level at which the physical control input appears is reached. This recursive HOCBF construction is introduced next.

3.3 Recursive HOCBF Construction and Safety Condition

Definition 3 (Recursive HOCBF Quantities) Starting from $H(\boldsymbol{x})$, the HOCBF recursion is defined as

$$\psi_0(\boldsymbol{x}) = H(\boldsymbol{x}), \qquad \psi_i(\boldsymbol{x}) = \dot{\psi}_{i-1}(\boldsymbol{x}) + \alpha_i(\psi_{i-1}(\boldsymbol{x})), \quad i = 1, \dots, r, \tag{10}$$

where α_i are sufficiently differentiable class-$\mathcal{K}$ functions. Their definition and regularity requirements are given in Appendix A.1. For the class-$\mathcal{K}$ function α_i, a simple choice can for example be the linear function $\alpha_i(\psi_{i-1}) = \gamma_i \psi_{i-1}$ with the constant parameter $\gamma_i > 0$.

For $i = 1$, Eq. (10) gives $\psi_1 = \dot{\psi}_0 + \alpha_1(\psi_0) = \dot{H} + \alpha_1(H)$. For a safety function of relative degree r, the physical control input first appears in ψ_r, as shown in Appendix A.2, and the HOCBF condition is

$$\psi_r(\boldsymbol{x}, \boldsymbol{u}) \geq 0. \tag{11}$$

Why this condition guarantees preservation of the original safety constraint is established by the forward-invariance result considered next.

3.4 Forward-Invariance Result

The HOCBF condition in Eq. (11) is used to ensure that the recursive safety conditions remain satisfied over time and subsequently the original safety condition is $H(\boldsymbol{x}) \geq 0$, and therefore $y \leq y_{\max}$. For a safety function $H(\boldsymbol{x}) = \psi_0$ of relative degree r, this requires that the initial state $\boldsymbol{x}(t_0)$ satisfies

$$\psi_i(\boldsymbol{x}(t_0)) \geq 0, \qquad i = 0, \dots, r-1. \tag{12}$$

Theorem 1 (Forward Invariance and Output Safety) *Consider the input-affine system in Eq. (4) and a safety function $H(\boldsymbol{x})$ of relative degree r. Let the functions α_i satisfy the class-$\mathcal{K}$ and regularity requirements given in Appendix A.1. If the initial condition satisfies Eq. (12) and a Lipschitz-continuous control input $\boldsymbol{u}$ satisfies the HOCBF condition*

$$\psi_r(\boldsymbol{x}, \boldsymbol{u}) \geq 0, \qquad \forall\, t \geq t_0, \tag{13}$$

then

$$\psi_i(\boldsymbol{x}(t)) \geq 0, \qquad i = 0, \dots, r-1, \qquad \forall\, t \geq t_0. \tag{14}$$

In particular, since $\psi_0 = H$,

$$H(\boldsymbol{x}(t)) \geq 0 \iff y(t) \leq y_{\max}, \qquad \forall\, t \geq t_0. \tag{15}$$

Proof The proof is given in Appendix A.5. □

Hence, if the recursive HOCBF conditions are satisfied initially and the HOCBF condition in Eq. (13) is enforced, the protected output cannot cross the physical output limit $y_{\max}$.

3.5 Resulting Control Constraint

The forward-invariance result shows that safety is guaranteed if the final HOCBF condition $\psi_r(\boldsymbol{x}, \boldsymbol{u}) \geq 0$ is satisfied. The remaining question is therefore how this condition restricts the physical control input.

Using the form of ψ_r, Eq. (110), derived in Appendix A.2 gives

$$\psi_r = a_r(\boldsymbol{x}) + b_r(\boldsymbol{x})\boldsymbol{u} + \Phi_r\left(H, \dot{H}, \ldots, H^{(r-1)}\right) \geq 0. \tag{16}$$

Here, $a_r(\boldsymbol{x})$ and $b_r(\boldsymbol{x})$ result from the r-th derivative of H according to Eq. (9), while Φ_r collects the additional terms generated by the HOCBF recursion, as derived in Appendix A.2.

Rearranging Eq. (16) gives the input control constraint

$$b_r(\boldsymbol{x})\boldsymbol{u} \geq -a_r(\boldsymbol{x}) - \Phi_r\left(H, \dot{H}, \ldots, H^{(r-1)}\right). \tag{17}$$

If the nominal input would violate Eq. (17), the limiting value lies on the active boundary of the HOCBF constraint, obtained by replacing the inequality in Eq. (17) by equality. For a scalar input, this equality can be solved directly for u if $b_r(\boldsymbol{x}) \neq 0$. For vector-valued inputs, any input satisfying the equality lies on the active boundary; a particular solution may, for example, be obtained using a pseudoinverse or an additional control-allocation criterion.

More generally, the admissible control input is often selected by solving a quadratic program that minimizes the deviation from the nominal control command while enforcing Eq. (17). A common objective is

$$\min_{\boldsymbol{u}} \|\boldsymbol{u} - \boldsymbol{u}_{\text{nom}}\|^2 \qquad \text{subject to Eq. (17).} \tag{18}$$

Here, $\boldsymbol{u}_{\text{nom}}$ denotes the control command generated by the nominal controller without safety modification. The optimization therefore preserves the nominal command whenever it satisfies the HOCBF constraint and modifies it only when required for safety.

4 Output Limiting Backstepping

In Output Limiting Backstepping the protection of a constrained system output is driven by specifying and designing a phase-plane boundary $\dot{y}_{\text{lim}}$ for the output rate $\dot{y}$. If the nominal response would violate this boundary, OLB limits the physical control input such that $\dot{y}$ follows the prescribed boundary $\dot{y}_{lim}$. The required limiting input is

obtained through a recursive backstepping construction. This section first introduces the physical phase-plane interpretation and motivates why this is an intuitive design metric. Afterwards the corresponding tracking problem and backstepping design is formulated.

4.1 Phase-Plane based Output Limiting

Output Limiting Backstepping first translates the physical output constraint introduced in Section 2 into a limit on the output rate. For the upper output limit $y_{\max}$, define the phase-plane boundary as

$$\dot{y}_{\lim} = \alpha_{\mathrm{OLB}}(y, y_{\max}). \tag{19}$$

The phase plane boundary in Eq. (19) specifies the maximum admissible output rate for each current value of y. Far from the physical limit, a comparatively large positive output rate may be allowed. As y approaches $y_{\max}$, the admissible rate can be reduced, with the boundary typically designed such that $\alpha_{\mathrm{OLB}}(y_{\max}, y_{\max}) = 0$.

The phase-plane boundary directly shapes the desired behavior of the protected output during limiting. With $\dot{y}_{\mathrm{nom}}$ denoting the output rate resulting from the nominal control, the following relations hold for the upper protection:

$$\begin{aligned} \dot{y}_{\mathrm{nom}} \leq \alpha_{\mathrm{OLB}}(y, y_{\max}) \quad &\Longrightarrow \quad \text{nominal control is retained,} \\ \dot{y}_{\mathrm{nom}} > \alpha_{\mathrm{OLB}}(y, y_{\max}) \quad &\Longrightarrow \quad \text{limiting becomes active \& } \dot{y} \to \alpha_{\mathrm{OLB}}(y, y_{\max}). \end{aligned} \tag{20}$$

Hence, OLB modifies the nominal control only when the nominal response would exceed the admissible phase-plane boundary. During active limiting, the control input is limited such that the actual output rate $\dot{y}$ follows the limiting rate $\dot{y}_{\lim} = \alpha_{\mathrm{OLB}}(y, y_{\max})$.

A simple choice for the phase-plane boundary is the linear relation

$$\dot{y}_{\lim} = \alpha_{\mathrm{OLB}}(y, y_{\max}) = \gamma_1 \left(y_{\max} - y\right), \qquad \gamma_1 > 0. \tag{21}$$

This form provides a direct time-domain interpretation of the phase-plane gain γ_1. Figure 1 illustrates one output response $y(t)$ during active limiting. Since active limiting aims to enforce $\dot{y} = \dot{y}_{\lim}$ the limiting rate $\dot{y}_{\lim}$ is, at each time instant, the slope of the tangent to the trajectory $y(t)$. If this tangent is extrapolated with constant slope until it reaches the physical output limit $y_{\max}$, the resulting predicted time to the limit is

$$\tau_p = \frac{y_{\max} - y}{\dot{y}_{\lim}} = \frac{y_{\max} - y}{\gamma_1 (y_{\max} - y)} = \frac{1}{\gamma_1}. \tag{22}$$

Equation (22) gives the following interpretation:

- At every time instant during active limiting, the tangent to $y(t)$ predicts the same remaining time τ_p to the physical limit.
- The actual trajectory does not reach $y_{\max}$ after τ_p, because Eq. (21) continuously reduces $\dot{y}_{\lim}$ as y approaches the limit.

- A larger γ_1 gives a smaller τ_p and therefore permits a faster approach toward $y_{\max}$, whereas a smaller γ_1 gives a slower approach.

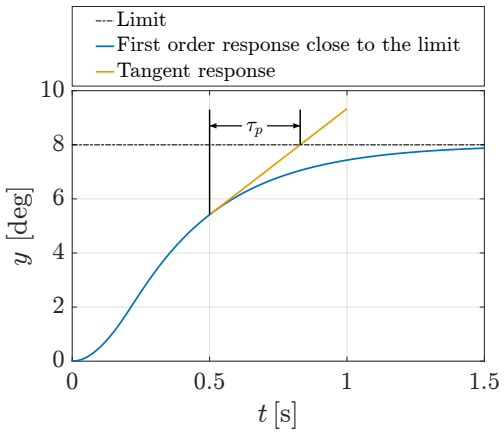


Fig. 1: Time-domain interpretation of the linear phase-plane boundary.

The phase-plane boundary need not be linear. One possible choice, used in the OLB formulation in Steffensen et al. (2019b), is a piecewise-polynomial phase-plane boundary; see Fig. 3. It is divided into different regions, each with a distinct purpose:

- Far from the physical limit: a first polynomial segment can allow comparatively large admissible rates toward the limit and therefore later intervention.
- Close to the physical limit: a second polynomial segment shapes the desired near-limit approach behavior and can be matched to the linear phase-plane behavior.
- Beyond the physical limit: an additional recovery segment prescribes a limiting rate directed back toward the admissible region, while its slope determines the aggressiveness of the recovery.

The advantages resulting from the additional shaping freedom of the piecewise-polynomial construction compared to a purely linear phase plane can be seen in Fig. 2. In the phase-plane plot on the right, the linear boundary is a straight line (green dashed) and the protection becomes active already at relatively small values of y, i.e. it is forced to trck the line. The system therefore enters the limiting regime early, even though it is still far from the physical limit $y_{\max}$.

The same effect is visible in the time response on the left. While the unprotected system would continue to follow the nominal response, the protected system can only approach $y_{\max}$ with some dynamics rather than switch abruptly to the limit. With the linear boundary, this approach starts early, causing an earlier deviation from the nominal response and a corresponding loss of maneuverability.

The piecewise-polynomial boundary allows this behavior to be shaped more freely. The protection can become active later, so that the system follows the nominal response for longer, while still enforcing the linear behavior close to $y_{\max}$. The response

can therefore remain more aggressive away from the limit and become sufficiently restrictive only near the boundary, reducing the loss of maneuverability caused by the protection and hence making it less conservative.

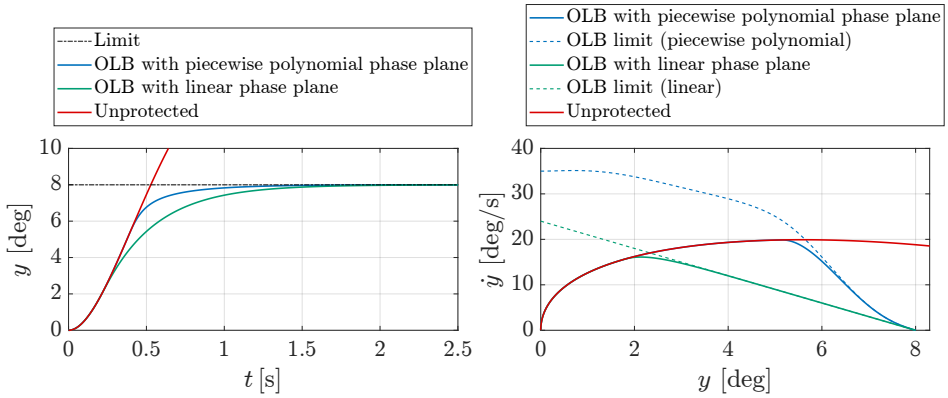


Fig. 2: Comparison of linear and piecewise-polynomial phase-plane limiting, based on Steffensen et al. (2019b). The piecewise-polynomial boundary permits larger output rates farther from the physical limit while retaining restrictive limiting behavior close to the boundary.

The phase-plane based protection design is attractive because the limiting behavior is specified in a physically interpretable way directly in the $(y, \dot{y})$ phase plane. The phase-plane boundary can therefore be used as a design object: the desired limiting and recovery behavior is chosen first from physical considerations, and the corresponding limiting control input is then constructed by the subsequent backstepping design.

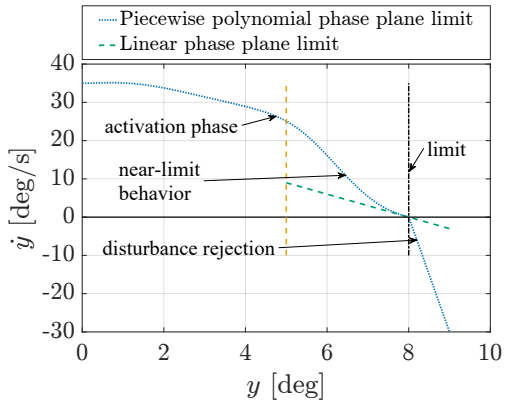


Fig. 3: Piecewise-polynomial phase-plane boundary and its different design regions, based on Steffensen et al. (2019b).

4.2 OLB System Structure and Tracking Problem

The OLB formulation is derived for a single-input system in strict-feedback form.

$$\begin{aligned}
\dot{\tilde{x}}_1 &= \tilde{f}_1(\tilde{x}_1) + \tilde{g}_1\tilde{x}_2, \\
\dot{\tilde{x}}_2 &= \tilde{f}_2(\tilde{x}_1, \tilde{x}_2) + \tilde{g}_2\tilde{x}_3, \\
&\vdots \\
\dot{\tilde{x}}_{r-1} &= \tilde{f}_{r-1}(\tilde{x}_1, \ldots, \tilde{x}_{r-1}) + \tilde{g}_{r-1}\tilde{x}_r, \\
\dot{\tilde{x}}_r &= \tilde{f}_r(\tilde{x}_1, \ldots, \tilde{x}_r) + \tilde{g}_r\tilde{u}.
\end{aligned} \tag{23}$$

where $\tilde{\boldsymbol{x}} = [\tilde{x}_1, \ldots, \tilde{x}_r]^{\mathrm{T}}$ are the states, $\tilde{u} \in \mathbb{R}$ is the physical control input and $\tilde{g}_i \neq 0$ are constant coefficients. Because of the strict feedback form $\tilde{x}_{i+1}$ enters the dynamics of $\tilde{x}_i$, while the physical input enters only the last state derivative. The protected output is the first physical state,

$$y = p(\tilde{\boldsymbol{x}}) = \tilde{x}_1. \tag{24}$$

As introduced in Section 4.1, during active limiting the output rate should follow the phase-plane boundary,

$$\dot{y} \to \dot{y}_{\mathrm{lim}} = \alpha_{\mathrm{OLB}}(y, y_{\mathrm{max}}). \tag{25}$$

In a standard backstepping tracking problem, the first physical state $\tilde{x}_1 = y$ follows a reference. Here, however, its derivative $\dot{\tilde{x}}_1 = \dot{y}$ should follow the limiting rate $\dot{y}_{\mathrm{lim}}$. Therefore, the following state transformation is introduced:

$$\begin{aligned}
x_i &= \dot{\tilde{x}}_i, \qquad i = 1, \ldots, r, \\
x_1 &= \dot{\tilde{x}}_1 = \dot{y}, \\
x_1 &\to \alpha_{\mathrm{OLB}}(y, y_{\mathrm{max}}).
\end{aligned} \tag{26}$$

The OLB problem is thus converted into a tracking problem for the transformed first state x_1. Its tracking error is

$$e_1 = \alpha_{\mathrm{OLB}}(y, y_{\mathrm{max}}) - x_1 = \dot{y}_{\mathrm{lim}} - \dot{y}. \tag{27}$$

Thus, $e_1 = 0$ means that the actual output rate is equal to the phase-plane limiting rate. The transformed system is derived in Appendix B.1 and can then be used for the recursive backstepping design, which is detailed next.

4.3 Recursive Backstepping and Limiting Control

The tracking error e_1 in Eq. (27) defines the first backstepping step. The remaining transformed states are then handled recursively. For $i = 2, \ldots, r-1$, define

$$e_i = x_{i,d} - x_i, \tag{28}$$

where $x_{i,d}$ is the desired value obtained in the preceding backstepping step. The recursive law can then be stated as follows.

Proposition 2 (OLB recursive backstepping law) *Consider the transformed strict-feedback system derived in Appendix B.1, repeated here for convenience:*

$$\begin{aligned} \dot{x}_1 &= f_1(x_1) + g_1 x_2, \\ \dot{x}_2 &= f_2(x_1, x_2) + g_2 x_3, \\ &\vdots \\ \dot{x}_{r-1} &= f_{r-1}(x_1, \ldots, x_{r-1}) + g_{r-1} x_r. \end{aligned} \tag{29}$$

For the quadratic Lyapunov candidate

$$V_i = \frac{1}{2} \sum_{j=1}^{i} e_j^2 \tag{30}$$

and the desired Lyapunov derivative

$$\dot{V}_i = -\sum_{j=1}^{i} c_j e_j^2, \qquad c_j > 0, \tag{31}$$

the corresponding recursive desired transformed states are obtained as follows.

The first desired transformed state is

$$x_{2,d} = \frac{1}{g_1} \left[\dot{\alpha}_{\mathrm{OLB}} - f_1(x_1) + c_1 e_1 \right]. \tag{32}$$

For $i = 2, \ldots, r-1$, the subsequent desired transformed states are obtained recursively as

$$x_{i+1,d} = \frac{1}{g_i} \left[\dot{x}_{i,d} - f_i(x_1, \ldots, x_i) + g_{i-1} e_{i-1} + c_i e_i \right]. \tag{33}$$

The recursion gives the final desired transformed state $x_{r,d}$. The proof is given in Appendix B.2.

The desired value $x_{r,d}$ is not the physical control input. From the state transformation in Eq. (26), $x_r = \dot{\tilde{x}}_r$. Using the last subsystem of the physical system in Eq. (23), the physical input must be chosen such that $x_r = x_{r,d}$, i.e.,

$$x_r = \dot{\tilde{x}}_r = \tilde{f}_r(\tilde{x}_1, \ldots, \tilde{x}_r) + \tilde{g}_r \tilde{u} \stackrel{!}{=} x_{r,d}. \tag{34}$$

Solving Eq. (34) for $\tilde{u}$ gives the OLB limiting input

$$\tilde{u}_{\mathrm{lim}}^{\mathrm{OLB}} = \frac{1}{\tilde{g}_r} \left[x_{r,d} - \tilde{f}_r(\tilde{x}_1, \ldots, \tilde{x}_r) \right]. \tag{35}$$

The quantity $\tilde{u}_{\mathrm{lim}}^{\mathrm{OLB}}$ is a limiting value, not a continuously applied control command. The nominal input is retained while the nominal response remains inside the admissible phase-plane region, i.e., while $\dot{y} \leq \dot{y}_{\mathrm{lim}}$. If the nominal input would exceed $\tilde{u}_{\mathrm{lim}}^{\mathrm{OLB}}$ it would produce $\dot{y} > \dot{y}_{\mathrm{lim}}$. It is therefore limited to the boundary value $\tilde{u}_{\mathrm{lim}}^{\mathrm{OLB}}$. At this value, $x_r = x_{r,d}$, and the backstepping construction makes the output rate follow the phase-plane boundary $\dot{y} = \dot{y}_{\mathrm{lim}}$.

Table 1: Clarification of potentially ambiguous notation.

Symbol	Meaning
α	Angle of attack ($y = \alpha$)
$\alpha_{\max}$	Maximum admissible angle of attack
α_{OLB}	OLB phase-plane boundary ($\dot{y}_{\lim}$)
α_i	HOCBF class-$\mathcal{K}$ functions
γ_1^{OLB}	Linear OLB phase-plane gain
$\gamma_1^{\mathrm{HOCBF}}$	First linear HOCBF class-$\mathcal{K}$ gain
γ_i, $i \geq 2$	Higher-order HOCBF gains

5 Comparison of OLB and HOCBF in the Single Recursion Case: Angle-of-Attack Protection

Notation clarification. Since the symbol α is used for different quantities, Table 1 summarizes the potentially ambiguous notation used in the following.

The OLB phase-plane boundary α_{OLB} and the HOCBF class-$\mathcal{K}$ functions α_i are design functions. Their gains are independent unless the derived correspondence conditions are imposed.

5.1 System and Protection Problem

To illustrate the relation between HOCBF and OLB, consider the linear short-period aircraft model

$$\dot{\alpha} = Z_\alpha \alpha + (1 + Z_q) q, \qquad \dot{q} = M_\alpha \alpha + M_q q + M_\eta \eta. \tag{36}$$

where α is the angle of attack, q is the pitch rate, and η is the elevator deflection. The model coefficients Z_α, Z_q, M_α, M_q, and M_η are constants, given in Table 2. The protected output and its upper limit are

$$y = \alpha, \qquad y_{\max} = \alpha_{\max}, \qquad \alpha \leq \alpha_{\max}. \tag{37}$$

The elevator input does not appear in $\dot{\alpha}$. Differentiating the first relation in Eq. (36) and substituting the pitch-rate dynamics $\dot{q}$ gives

$$\begin{aligned} \ddot{\alpha} &= Z_\alpha \dot{\alpha} + (1 + Z_q) \dot{q} \\ &= Z_\alpha \dot{\alpha} + (1 + Z_q) \left(M_\alpha \alpha + M_q q + M_\eta \eta \right). \end{aligned} \tag{38}$$

Hence, provided that $(1 + Z_q) M_\eta \neq 0$, the physical input first appears in $\ddot{\alpha}$.

For the HOCBF formulation, the short-period model in Eq. (36) has the input-affine form defined in Eq. (4), with

$$\boldsymbol{x} = \begin{bmatrix} \alpha \\ q \end{bmatrix}, \qquad \boldsymbol{f}(\boldsymbol{x}) = \begin{bmatrix} Z_\alpha \alpha + (1 + Z_q) q \\ M_\alpha \alpha + M_q q \end{bmatrix}, \qquad \boldsymbol{g}(\boldsymbol{x}) = \begin{bmatrix} 0 \\ M_\eta \end{bmatrix}, \qquad u = \eta. \tag{39}$$

Table 2: Plant, and nominal NDI controller parameters.

Plant and actuator		Nominal NDI controller	
Parameter	Value	Parameter	Value
Z_α	-1.38	ω_{ref}	4
Z_q	0	ζ_{ref}	0.8
M_α	-4.588	K_α	81
M_q	-2	$K_{\dot\alpha}$	18
M_η	-4		

The error-controller gains are calculated as $K_\alpha = \omega_{\text{e}}^2$ and $K_{\dot\alpha} = 2\zeta_{\text{e}}\omega_{\text{e}}$, corresponding to $\omega_{\text{e}} = 9$ and $\zeta_{\text{e}} = 1$.

For the OLB formulation, the short-period model has the triangular structure defined in Eq. (23),

$$\begin{aligned} \dot\alpha &= \underbrace{Z_\alpha \alpha}_{\tilde f_1} + \underbrace{(1 + Z_q)}_{\tilde g_1} q, \\ \dot q &= \underbrace{M_\alpha \alpha + M_q q}_{\tilde f_2} + \underbrace{M_\eta}_{\tilde g_2} \eta. \end{aligned} \tag{40}$$

Hence, $\tilde x_1 = \alpha$, $\tilde x_2 = q$, and $\tilde u = \eta$. Applying the state transformation in Eq. (26), $x_1 = \dot\alpha$ and $x_2 = \dot q$, gives the transformed system, according to Eq. (29), required for the recursive step,

$$\begin{aligned} \dot x_1 = \ddot\alpha &= \underbrace{Z_\alpha x_1}_{f_1(x_1)} + \underbrace{(1 + Z_q)}_{g_1} x_2, \\ x_2 = \dot q &= M_\alpha \alpha + M_q q + M_\eta \eta. \end{aligned} \tag{41}$$

The second line of Eq. (41) is retained in its physical form because, according to the OLB limiting-input construction in Eq. (34), the final transformed desired state $x_{2,d} = \dot q_d$ is used directly to determine the physical elevator input.

5.2 Protection Design Choices

The following definition introduces the linear design choices used to compare the two methods. Then the conditions required for the correspondence of both methods are derived.

Definition 4 (Linear HOCBF and OLB designs) For OLB, we choose the linear phase-plane limit in Eq. (21),

$$\dot\alpha_{\text{lim}} = \alpha_{\text{OLB}}(\alpha, \alpha_{\max}) = \gamma_1^{\text{OLB}}(\alpha_{\max} - \alpha), \qquad \gamma_1^{\text{OLB}} > 0, \tag{42}$$

and define the first OLB tracking error as

$$e_1 = \dot\alpha_{\text{lim}} - \dot\alpha. \tag{43}$$

Let $c_1 > 0$ denote the first OLB backstepping gain, that will be used later.

For HOCBF, we choose the safety function H according to the simple choice introduced in Definition 1

$$H(\boldsymbol{x}) = h(\alpha) = \alpha_{\max} - \alpha = \psi_0, \tag{44}$$

together with the linear class-$\mathcal{K}$ function choice introduced in Definition 3

$$\alpha_1(H) = \gamma_1^{\text{HOCBF}}\psi_0 = \gamma_1^{\text{HOCBF}}(\alpha_{max} - \alpha), \quad \alpha_2(\psi_1) = \gamma_2\psi_1, \quad \gamma_1^{\text{HOCBF}} > 0, \quad \gamma_2 > 0. \tag{45}$$

Notably, the chosen HOCBF α_1 class-$\mathcal{K}$ function and the OLB limiting phase plane $\dot{\alpha}_{lim} = \alpha_{OLB}(\alpha, \alpha_{max})$ correspond to each other if $\gamma_1^{\text{HOCBF}} = \gamma_1^{\text{OLB}}$.

5.3 Protection Laws

5.3.1 HOCBF Protection Law

Since the safety function in the present example has relative degree $r = 2$, the HOCBF limiting input is obtained from Eq. (16) as

$$\eta_{\text{lim}}^{\text{HOCBF}} = \frac{-a_2(\boldsymbol{x}) - \Phi_2(H, \dot{H})}{b_2(\boldsymbol{x})}. \tag{46}$$

To evaluate Eq. (46), the terms $a_2(\boldsymbol{x})$ and $b_2(\boldsymbol{x})$ are obtained from the second derivative of the safety function $\ddot{H} = a_2(\boldsymbol{x}) + b_2(\boldsymbol{x})u$, according to Eq.(109). With

$$H = \alpha_{\max} - \alpha, \qquad \dot{H} = -\dot{\alpha}, \qquad \ddot{H} = -\ddot{\alpha}, \tag{47}$$

and using the short-period dynamics in Eq. (38), this gives

$$\begin{aligned} \ddot{H} &= -\ddot{\alpha} \\ &= \underbrace{-Z_\alpha\dot{\alpha} - (1 + Z_q)(M_\alpha\alpha + M_q q)}_{a_2(\boldsymbol{x})} + \underbrace{-(1 + Z_q)M_\eta}_{b_2(\boldsymbol{x})}\eta. \end{aligned} \tag{48}$$

The remaining term in Eq. (46) is $\Phi_2(H, \dot{H})$, which follows from the HOCBF recursion in Eq. (10). For the present case,

$$\psi_0 = H, \qquad \psi_1 = \dot{\psi}_0 + \alpha_1(\psi_0) = \dot{H} + \gamma_1^{\text{HOCBF}}H, \tag{49}$$

where $\alpha_1(\psi_0)$ as defined in Eq.(45) was used and

$$\psi_2 = \dot{\psi}_1 + \alpha_2(\psi_1) = \ddot{H} + \gamma_1^{\text{HOCBF}}\dot{H} + \gamma_2\psi_1 = \ddot{H} + (\gamma_1^{\text{HOCBF}} + \gamma_2)\dot{H} + \gamma_1^{\text{HOCBF}}\gamma_2 H. \tag{50}$$

Thus, the recursion term is according to Eq.(108)

$$\Phi_2(H, \dot{H}) = (\gamma_1^{\text{HOCBF}} + \gamma_2)\dot{H} + \gamma_1^{\text{HOCBF}}\gamma_2 H. \tag{51}$$

Figure 4 visualizes the corresponding block diagram.

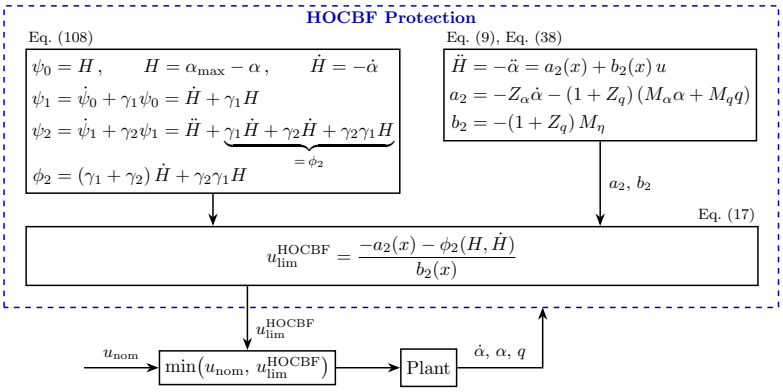


Fig. 4: Implementation of the HOCBF protection law for the short-period angle-of-attack protection example.

5.3.2 OLB Protection Law

The OLB limiting input is obtained from Eq. (35). For the present case, $r = 2$ and $\tilde{u} = \eta$, such that

$$\eta_{\lim}^{\mathrm{OLB}} = \frac{1}{\tilde{g}_2}\left[x_{2,d} - \tilde{f}_2\right]. \tag{52}$$

According to Eq. (40), $\tilde{f}_2 = M_\alpha\alpha + M_q q, \tilde{g}_2 = M_\eta$. The quantity $x_{2,d}$ follows from Eq. (32) as

$$x_{2,d} = \frac{1}{g_1}\left[\dot{\alpha}_{\mathrm{OLB}} - f_1(x_1) + c_1 e_1\right]. \tag{53}$$

According to Eq. (41), $f_1(x_1) = Z_\alpha\dot{\alpha}, g_1 = 1 + Z_q$. Furthermore, with the phase-plane limit defined in Eq. (42),

$$e_1 = \alpha_{\mathrm{OLB}}(\alpha, \alpha_{\max}) - \dot{\alpha} = \gamma_1^{\mathrm{OLB}}(\alpha_{\max} - \alpha) - \dot{\alpha}, \qquad \dot{\alpha}_{\mathrm{OLB}} = -\gamma_1^{\mathrm{OLB}}\dot{\alpha}. \tag{54}$$

Figure 5 visualizes the corresponding block diagram.

5.4 HOCBF-OLB Correspondence

With the design choices in Definition 4, the following correspondences between HOCBF and OLB can now be shown.

Proposition 3 (HOCBF-OLB correspondence for linear design and relative degree two protections) *Consider the short-period system in Eq. (36) with the angle-of-attack constraint in Eq. (37). Let the OLB and HOCBF designs be linear as given by Definition 4.*

1. Phase-plane and recursive-quantity correspondence. *If*

$$\boxed{\gamma_1^{\mathrm{OLB}} = \gamma_1^{\mathrm{HOCBF}},} \tag{55}$$

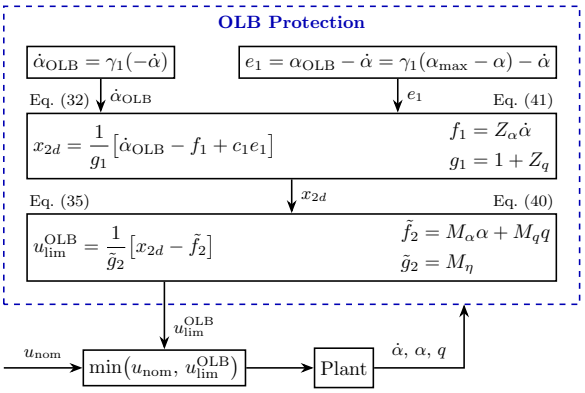


Fig. 5: Implementation of the OLB protection law for the short-period angle-of-attack protection example.

then

$$\boxed{\psi_1 = e_1.} \tag{56}$$

Thus, with the same gain γ_1, the first HOCBF recursive quantity Ψ_1 and the OLB phase-plane tracking error are identical. Consequently, Ψ_1 can be interpreted as the tracking error e_1 between $\dot{\alpha}_{lim}$ and $\dot{\alpha}$.

The HOCBF condition $\psi_1 \geq 0$ and the OLB phase-plane limit describe then the same rate limit,

$$\boxed{\dot{\alpha} \leq \gamma_1^{\mathrm{OLB}}(\alpha_{\max} - \alpha) = \gamma_1^{\mathrm{HOCBF}}(\alpha_{\max} - \alpha) = \dot{\alpha}_{\mathrm{lim}}.} \tag{57}$$

In particular, their common phase-plane boundary is

$$\dot{\alpha} = \dot{\alpha}_{\mathrm{lim}}. \tag{58}$$

The relations in Eqs. (56)–(58) are independent of the OLB gain c_1 and the HOCBF gain γ_2.

2. Active error-dynamics correspondence. *We already established $\Psi_1 = e_1$. We now compare the dynamics of the error e_1 during active limiting for both methods. If, in addition to Eq. (55),*

$$\boxed{c_1 = \gamma_2,} \tag{59}$$

then the active HOCBF boundary and the active OLB limiting law give

$$\boxed{\dot{\psi}_1 = -\gamma_2 \psi_1 = \dot{e}_1 = -c_1 e_1}. \tag{60}$$

The HOCBF active boundary and the active OLB limiting law therefore give the same error dynamics for tracking $\dot{\alpha}_{\mathrm{lim}}$.

3. Limiting-control correspondence. *Under both matching conditions in Eqs. (55) and (59), the limiting elevator inputs obtained from HOCBF and OLB are identical,*

$$\boxed{\eta_{\mathrm{lim}}^{\mathrm{HOCBF}} = \eta_{\mathrm{lim}}^{\mathrm{OLB}}.} \tag{61}$$

Denoting the common value of γ_1^{OLB} and $\gamma_1^{\mathrm{HOCBF}}$ by γ_1, the common limiting input is

$$\boxed{\eta_{\mathrm{lim}} = \frac{-(Z_\alpha + \gamma_1 + \gamma_2)\dot{\alpha} - (1 + Z_q)(M_\alpha \alpha + M_q q) + \gamma_1 \gamma_2 (\alpha_{\max} - \alpha)}{(1 + Z_q) M_\eta}.} \tag{62}$$

The three statements are proved in Appendix C.

5.5 Reference Model and Nominal Controller

The commanded angle of attack α_{cmd} is passed through a second-order reference model,

$$G_{\mathrm{ref}}(s) = \frac{\alpha_{\mathrm{ref}}(s)}{\alpha_{\mathrm{cmd}}(s)} = \frac{\omega_{\mathrm{ref}}^2}{s^2 + 2\zeta_{\mathrm{ref}}\omega_{\mathrm{ref}}s + \omega_{\mathrm{ref}}^2}, \tag{63}$$

with ω_{ref} and ζ_{ref} as in Table 2. The reference model provides α_{ref}, $\dot{\alpha}_{\mathrm{ref}}$, and $\ddot{\alpha}_{\mathrm{ref}}$.

A dynamic-inversion controller is used to track the reference trajectory. Inverting the angle-of-attack dynamics in Eq. (38) gives the nominal elevator command

$$\eta_{\mathrm{nom}} = \frac{\ddot{\alpha}_{\mathrm{des}} - Z_\alpha\dot{\alpha} - (1+Z_q)\,(M_\alpha\alpha + M_q q)}{(1+Z_q)M_\eta}. \tag{64}$$

The desired angle-of-attack acceleration is defined as

$$\ddot{\alpha}_{\mathrm{des}} = \ddot{\alpha}_{\mathrm{ref}} + K_{\dot{\alpha}}\,(\dot{\alpha}_{\mathrm{ref}} - \dot{\alpha}) + K_\alpha\,(\alpha_{\mathrm{ref}} - \alpha)\,, \tag{65}$$

with $K_{\dot{\alpha}}$ and K_α as in Table 2.

5.6 Simulation Results

The protection laws derived above were implemented according to the block diagrams in Figs. 4 and 5. A constant angle-of-attack command of $\alpha_{\mathrm{cmd,raw}} = 15\,\mathrm{deg}$, which exceeds the protection limit $\alpha_{\max} = 10\,\mathrm{deg}$, is applied at $t = 1\,\mathrm{s}$. For comparison, the unprotected system and a simple command saturation, $\alpha_{\mathrm{cmd}} = \min(\alpha_{\mathrm{cmd,raw}}, \alpha_{\max})$, are also simulated.

For HOCBF and OLB, the parameters are matched according to Proposition 3. Two choices, $\gamma_1^{\mathrm{OLB}} = \gamma_1^{\mathrm{HOCBF}} = 5$ and $\gamma_1^{\mathrm{OLB}} = \gamma_1^{\mathrm{HOCBF}} = 22$, are considered, while $\gamma_2 = c_1 = 22$ is used in both cases.

Figure 6(a) shows the resulting angle-of-attack responses. Without protection, α follows the commanded value and therefore exceeds $\alpha_{\max}$. All protected cases remain below the prescribed limit. For both values of γ_1, the HOCBF and OLB responses coincide, as expected from the analytical correspondence derived above. Increasing γ_1 allows a faster approach toward the limit. The simple command saturation also prevents an exceedance in this example, but results in a slower transient.

The phase-plane representation in Fig. 6(b) illustrates the influence of γ_1 more directly. The HOCBF and OLB approach the same limiting boundary $\dot{\alpha}_{\mathrm{lim}} = \gamma_1\,(\alpha_{\max} - \alpha)$. Increasing γ_1 steepens this boundary and therefore permits larger values of $\dot{\alpha}$ during the approach toward $\alpha_{\max}$. In contrast, command saturation does not explicitly prescribe the admissible output rate. Its phase-plane trajectory crosses the $\gamma_1 = 5$ limiting boundary in this example. Command saturation provides no direct design freedom over the desired approach rate toward the constraint.

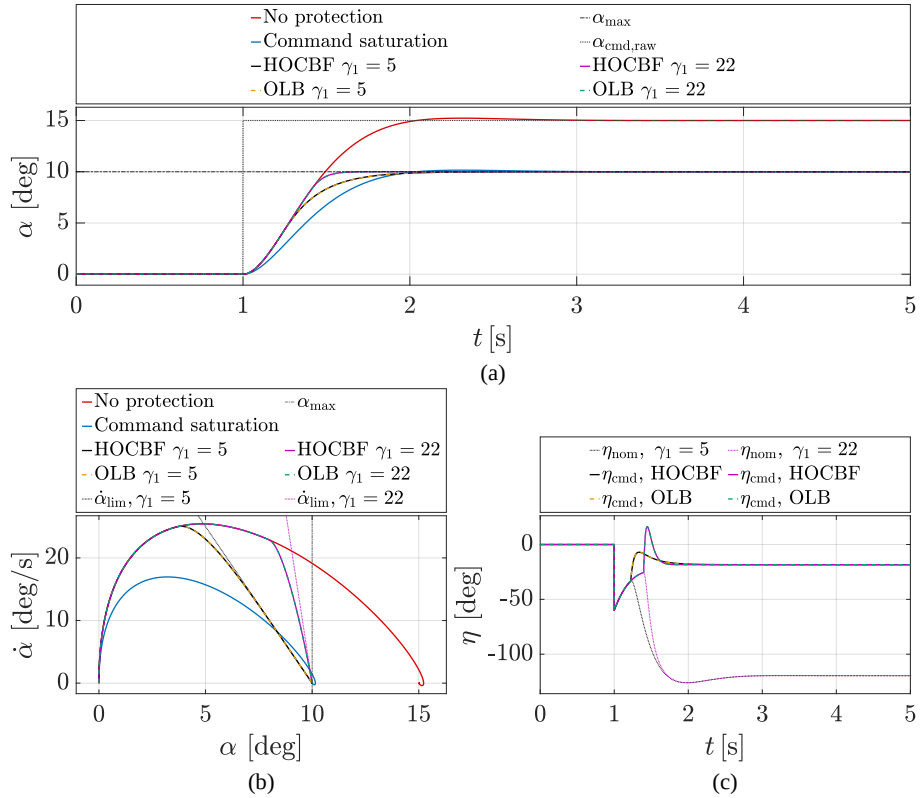


Fig. 6: Simulation results for an angle-of-attack command above the prescribed limit.

Figure 6(c) shows the corresponding elevator commands. Here, η_{nom} denotes the nominal elevator command generated by the controllerbefore beeing limited by η_{lim} which is computed by the protection law. Due to the sign of the elevator effectiveness $M_\eta < 0$, an increasingly negative elevator deflection increases the angle of attack. Consequently, η_{lim} represents a lower bound on the admissible elevator command in the present example, such that

$$\eta_{\mathrm{cmd}} = \max\left(\eta_{\mathrm{nom}}, \eta_{\mathrm{lim}}\right). \tag{66}$$

Before activation of the protection, $\eta_{\mathrm{nom}} \geq \eta_{\mathrm{lim}}$ and the nominal command is retained. Once the nominal controller demands an elevator deflection below this bound, the protection becomes active and $\eta_{\mathrm{cmd}} = \eta_{\mathrm{lim}}$. The protection therefore makes the elevator command less negative, reducing the control action that drives the angle of attack toward larger values and thereby slowing the increase in α. As soon as the protection kicks in a difference between η_{nom} and η_{cmd} becomes visible. The nominal controller continues to try to track an angle-of-attack reference above the prescribed limit and

is unaware of the modified control input by the protection. The protected system cannot reach this reference, such that a tracking error remains and the nominal controller demands increasingly negative elevator deflections. The protection prevents this additional control action from being applied and instead keeps the commanded elevator at the limiting value η_{lim}. The influence of γ_1 is also visible in the control commands. For the smaller value $\gamma_1 = 5$, limiting starts earlier. For $\gamma_1 = 22$, the steeper phase-plane boundary permits a faster approach toward $\alpha_{\max}$ and therefore allows the nominal command to be retained for longer. Once limiting becomes active, a faster modification of the elevator command is required to reduce the angle-of-attack rate faster. The limiting commands η_{lim} obtained from HOCBF and OLB are identical and therefore lie exactly on top of each other. Accordingly, the protected commands η_{cmd} also coincide for HOCBF and OLB. The simulation therefore confirms the analytical correspondence not only at the level of the protected angle-of-attack response, but also directly at the level of the computed limiting control input.

Matching γ_1^{OLB} and $\gamma_1^{\mathrm{HOCBF}}$ leads to the same phase-plane boundary. Matching the additional gains c_1 and γ_2 makes the angle of attack response and the resulting limiting elevator input to coincide.

6 General Relation Between HOCBF and OLB

The short-period aircraft model example showed that HOCBF and OLB can produce the same phase-plane boundary, the same active error dynamics, and the same limiting physical input when their design parameters are matched. This raises the question whether this correspondence is specific to the considered example or whether it reflects a more general relation between the two methods.

Before comparing their mathematical constructions, it is important to distinguish their applicability. Table 3 summarizes the main structural differences for the HOCBF and OLB formulations considered in this paper.

The HOCBF formulation applies to a broader system class than the OLB formulation. In particular, HOCBF does not require the strict-feedback structure of Eq. (23) and can constrain vector-valued control inputs, whereas the OLB construction in Section 4 is formulated for a scalar physical input. The following mathematical comparison is therefore restricted to systems for which both formulations can be applied.

Despite this more restrictive system class, OLB provides several useful design features that are not immediately visible in the HOCBF formulation:

1. **Intuitive physical phase-plane design.** OLB specifies the desired limiting behavior directly through the physical phase-plane boundary

$$\dot{y}_{\mathrm{lim}} = \alpha_{\mathrm{OLB}}(y, y_{\max}).$$

   The admissible approach toward the output limit can therefore be selected from physical considerations before the corresponding limiting input is derived. For example, the phase-plane boundary may determine how fast the protected output

Table 3: General comparison of the HOCBF and OLB formulations considered in this paper.

Aspect	**HOCBF**	**OLB**
System structure	Nonlinear input-affine system	Strict-feedback system
Physical control input	Scalar or vector-valued input	Scalar input
Protected output	Scalar output $y = p(\boldsymbol{x})$	First physical state $y = \tilde{x}_1$
Design construction	Safety function $H(\boldsymbol{x}) = h(p(\boldsymbol{x}))$ and class-$\mathcal{K}$ functions α_i in the recursive HOCBF construction	Backstepping tracking problem for the designed limiting output rate $\dot{y}_{\text{lim}} = \alpha_{\text{OLB}}(y, y_{\max})$, using Lyapunov functions, desired error dynamics, and negative-semidefinite Lyapunov-function derivatives
Associated guarantee	Forward invariance of the safe set when the HOCBF conditions and required initial conditions are satisfied	Lyapunov-based stability and convergence of the tracking-error dynamics under the active limiting law
Result of the construction	Constraint on the physical control input and corresponding **admissible input set**	Active **limiting value** of the physical control input

may approach its limit as a function of the remaining distance to that limit. The resulting limiting behavior therefore has a direct physical interpretation.

2. **Shaping with piecewise-polynomial construction.** As introduced in Section 4.1, the phase-plane boundary is not restricted to a linear relation. The piecewise-polynomial construction allows additional physical constraints and design objectives to be incorporated directly into the desired limiting behavior. Different regions can, for example, be used to shape different behavior for how the output approaches the limit close to the boundary or when far away from it, and how the system should recover after the limit has been exceeded.
3. **Lyapunov-based construction of the active limiting dynamics.** The OLB limiting law is obtained through the recursive backstepping design using Lyapunov functions and desired tracking-error dynamics. This establishes stability and convergence of the tracking errors toward the designed limiting behavior when the protection or limiting law is active.

The first two points are useful because they allow to design the desired protection behavior in physically meaningful quantities. Additional physical constraints or design objectives can be incorporated directly into how the protected output approaches and, if necessary, recovers after limit violation, rather than this behavior arising only indirectly from design parameter tuning. The third point provides a Lyapunov-based stability result for tracking the selected limiting behavior.

These properties motivate the general comparison. The following analysis investigates whether the physically interpretable OLB design can be transferred to HOCBF while retaining the broader HOCBF admissible-set formulation. In particular, we ask:

1. Under which conditions do HOCBF and OLB define the same physical phase-plane boundary and what relation then holds between the first HOCBF recursive quantity and the first OLB tracking error?
2. Does this correspondence remain valid when additional recursive levels are required?
3. Which additional relations are required for the same higher-order active limiting behavior and, ultimately, the same limiting physical input?

To answer these questions, we first compare the phase-plane boundary and the first recursive quantities. We then investigate how the correspondence changes at higher order.

6.1 First-Level Correspondence

This section investigates under which conditions HOCBF and OLB define the same physical phase-plane boundary and what relation then holds between the first HOCBF recursive quantity and the first OLB tracking error.

Proposition 4 (General phase-plane and first-quantity correspondence) *Consider a system for which both HOCBF and OLB can be applied to the same protected output*

$$y = p(\boldsymbol{x}) \leq y_{\max}. \tag{67}$$

Let the HOCBF safety function be

$$H(\boldsymbol{x}) = h(y = p(\boldsymbol{x})), \qquad \frac{\partial h}{\partial y} < 0 \tag{68}$$

and let the OLB phase-plane boundary be

$$\dot{y}_{\text{lim}}^{\text{OLB}} = \alpha_{\text{OLB}}(y, y_{\max}). \tag{69}$$

Then the HOCBF and OLB formulations define the same physical phase-plane boundary, i.e. $\dot{y}_{\text{lim}}^{\text{OLB}} = \dot{y}_{\text{lim}}^{\text{HOCBF}}$ *if the first HOCBF class-$\mathcal{K}$ function satisfies*

$$\boxed{\alpha_1(h(y)) = -\frac{\partial h}{\partial y}\alpha_{\text{OLB}}(y, y_{\max}).} \tag{70}$$

For Eq. (70) to define a valid HOCBF design, its right-hand side must be expressible as a class-$\mathcal{K}$ function of $h(y)$ and must satisfy the regularity requirements of the subsequent HOCBF recursion.

Under the phase-plane mapping in Eq. (70), the first HOCBF quantity ψ_1 and the first OLB tracking error

$$e_1 = \dot{y}_{\text{lim}}^{\text{OLB}} - \dot{y} \tag{71}$$

are related by

$$\boxed{\psi_1 = -\frac{\partial h}{\partial y}\, e_1}. \tag{72}$$

For an affine safety function

$$h(y) = k\,(y_{\max} - y)\,, \qquad k > 0, \tag{73}$$

Eq. (72) reduces to

$$\psi_1 = k\, e_1. \tag{74}$$

The proof is given in Appendix D.1.

The phase-plane correspondence in Eq. (70) does not require a linear OLB phase-plane boundary. The function $\alpha_{\mathrm{OLB}}(y, y_{\max})$ may therefore also represent the nonlinear or piecewise-polynomial boundary introduced in Section 4.1, provided that Eq. (70) results in a valid HOCBF class-$\mathcal{K}$ function α_1. Thus, the physical limiting behavior can first be designed in the $(y, \dot{y})$ phase plane and then be mapped to the HOCBF design quantities. For the simple safety function in Eq. (73), the scaling between ψ_1 and e_1 is constant.

This establishes the correspondence at the first recursive level. It does not yet imply that the subsequent HOCBF and OLB recursions also coincide. This is investigated next.

6.2 Higher-Order Correspondence

The phase-plane mapping, Eq. (70), established in the preceding subsection ensures that HOCBF and OLB impose the same output-rate boundary $\dot{y}_{\mathrm{lim}}$. However, this does not yet imply that the subsequent recursive quantities also describe the same active higher-order behavior. The following proposition states the additional conditions required for this correspondence.

Proposition 5 (Higher-order HOCBF–OLB correspondence) *Assume that the phase-plane mapping of Eq. (70) is satisfied and that the first quantities are therefore, according to Eq. (72), related by*

$$\psi_1 = -\frac{\partial h}{\partial y} e_1. \tag{75}$$

(i) ***General nonlinear safety function.*** *For a general nonlinear safety function $h(y)$, differentiation of Eq. (75) gives*

$$\dot{\psi}_1 = -\frac{\mathrm{d}}{\mathrm{d}t}\left(\frac{\partial h}{\partial y}\right) e_1 - \frac{\partial h}{\partial y}\dot{e}_1. \tag{76}$$

For the safety function

$$h(y) = k\,(y_{\max} - y)\,, \qquad k > 0, \tag{77}$$

the additional term in Eq. (76) vanishes such that a correspondence of the subsequent dynamics is established

$$\psi_1 = k e_1, \qquad \dot{\psi}_1 = k\dot{e}_1. \tag{78}$$

However, according to Eq. (76) a general correspondence of the subsequent HOCBF and OLB dynamics is not implied by the equality of the physical phase-plane boundary, $\dot{y}_{\mathrm{lim}}^{\mathrm{OLB}} = \dot{y}_{\mathrm{lim}}^{\mathrm{HOCBF}}$ through Eq. (75) alone.

(ii) ***Higher-order active error-dynamics correspondence.***
For the safety function in Eq. (77), the following higher-order correspondences hold.

(a) ***One OLB backstepping recursion.***
Let the next HOCBF class-$\mathcal{K}$ function be linear,

$$\alpha_2(\psi_1) = \gamma_2 \psi_1, \qquad \gamma_2 > 0. \tag{79}$$

Then the active HOCBF boundary $\psi_2 = 0$ reproduces the OLB desired first-error dynamics

$$\dot{e}_1 = -c_1 e_1, \qquad c_1 > 0, \tag{80}$$

with $e_1 = \dot{y}_{\text{lim}} - \dot{y}$, if

$$\boxed{\gamma_2 = c_1}. \tag{81}$$

This is what we obtained already for the short-period example.

(b) ***Two OLB backstepping recursions.***
Let the subsequent HOCBF class-$\mathcal{K}$ functions be

$$\alpha_2(\psi_1) = \gamma_2 \psi_1, \qquad \alpha_3(\psi_2) = \gamma_3 \psi_2, \qquad \gamma_2, \gamma_3 > 0. \tag{82}$$

On the active HOCBF boundary $\psi_3 = 0$, the resulting dynamics of the first error are

$$\ddot{e}_1 + (\gamma_2 + \gamma_3)\dot{e}_1 + \gamma_2 \gamma_3 e_1 = 0. \tag{83}$$

For OLB the resulting dynamics of e_1 are

$$\ddot{e}_1 + (c_1 + c_2)\dot{e}_1 + \left(c_1 c_2 + g_1^2\right) e_1 = 0. \tag{84}$$

Consequently, the active HOCBF and OLB error dynamics are identical if

$$\boxed{\begin{aligned} \gamma_2 + \gamma_3 &= c_1 + c_2, \\ \gamma_2 \gamma_3 &= c_1 c_2 + g_1^2. \end{aligned}} \tag{85}$$

Statement (i) follows directly from Eq. (76). Statement (ii) is proved in Appendix D.2. The main implications are as follows.

1. Equation (85) shows an important difference from the single-recursion case. The HOCBF gains are coupled through both OLB gains and the system coefficient g_1. Thus, the simple relation $\gamma_2 = c_1$ observed for one recursion does not extend as a direct one-to-one gain correspondence at higher order.
2. Though the affine choice of $h(y) = k\,(y_{\max} - y)$ is important for this result it shall be noted that it does not restrict the physical phase-plane boundary itself to be linear. α_1 can be chosen according to Eq. (70), as $\alpha_1 = -\frac{\partial h}{\partial y}\alpha_{\text{OLB}}(y, y_{\max})$ and a nonlinear or piecewise-polynomial function $\alpha_{\text{OLB}}(y, y_{\max})$ may still define the desired physical boundary. The affine safety function only removes the first term in Eq. (76), and by that allows the subsequent recursive dynamics to be matched.

7 Comparison in the Higher-Order Case: Angle-of-Attack Protection in the Presence of Actuator Dynamics

7.1 System and Protection Problem

The single-recursion example in Section 5 considers the elevator deflection η as the physical control input. We now extend the same short-period model by first-order elevator actuator dynamics. The protected output remains the angle of attack, while the commanded elevator deflection η_{cmd} becomes the physical input of the augmented system.

Using the short-period dynamics in Eq. (36), the augmented system is

$$\begin{aligned} \dot{\alpha} &= Z_\alpha \alpha + (1 + Z_q) q, \\ \dot{q} &= M_\alpha \alpha + M_q q + M_\eta \eta, \\ \dot{\eta} &= \frac{1}{\tau_\eta} \left(\eta_{\text{cmd}} - \eta \right), \qquad \tau_\eta > 0. \end{aligned} \tag{86}$$

where η is the actual elevator deflection and η_{cmd} is the commanded elevator deflection. The protected output and its upper limit remain those defined in Eq. (37), $y = \alpha$, $\alpha \leq \alpha_{\max}$.

The commanded elevator deflection does not appear in $\dot{\alpha}$ or $\ddot{\alpha}$, but appears in the third derivative of α,

$$\begin{aligned} \alpha^{(3)} &= Z_\alpha \dddot{\alpha} + (1 + Z_q) \ddot{q} = Z_\alpha \dddot{\alpha} + (1 + Z_q)(M_q \dot{q} + M_\alpha \dot{\alpha} + M_\eta \dot{\eta}) \\ &= Z_\alpha \dddot{\alpha} + (1 + Z_q)(M_q \dot{q} + M_\alpha \dot{\alpha} + M_\eta (\frac{1}{\tau_\eta} \left(\eta_{\text{cmd}} - \eta \right))). \end{aligned} \tag{87}$$

Hence, provided that $(1 + Z_q) M_\eta \neq 0$, the safety function has relative degree $r = 3$. Thus, the actuator dynamics add one recursive level compared with the single-recursion short-period example.

7.2 Protection Design Choices

For HOCBF, we choose again the safety function $H(\boldsymbol{x}) = \alpha_{\max} - \alpha = \psi_0$, and linear class-$\mathcal{K}$ functions $\alpha_i(\psi_i) = \gamma_i \psi_i$ with $\gamma_i > 0$.

For OLB, we choose again the linear phase-plane boundary $\dot{\alpha}_{\text{lim}} = \gamma_1^{\text{OLB}} \left(\alpha_{\max} - \alpha \right), \qquad \gamma_1^{\text{OLB}} > 0$ with tracking error $e_1 = \dot{\alpha}_{\text{lim}} - \dot{\alpha}$.

7.3 Protection Laws

7.3.1 HOCBF Protection Law

Since the safety function in the present example has relative degree $r = 3$, the HOCBF limiting input is obtained from Eq. (16) as

$$\eta_{\text{cmd,lim}}^{\text{HOCBF}} = \frac{-a_3(\boldsymbol{x}) - \Phi_3(H, \dot{H}, \ddot{H})}{b_3(\boldsymbol{x})}. \tag{88}$$

To evaluate Eq. (88), the terms $a_3(\boldsymbol{x})$ and $b_3(\boldsymbol{x})$ are obtained, according to Eq. (109), from the third derivative of the safety function. With

$$H = \alpha_{\max} - \alpha, \qquad \dot{H} = -\dot{\alpha}, \qquad \ddot{H} = -\ddot{\alpha}, \qquad H^{(3)} = -\alpha^{(3)}, \tag{89}$$

and using $\alpha^{(3)}$ from Eq. (87), this gives

$$H^{(3)} = \underbrace{-Z_\alpha \ddot{\alpha} - (1 + Z_q)\left(M_\alpha \dot{\alpha} + M_q \dot{q} - \frac{M_\eta}{\tau_\eta}\eta\right)}_{a_3(\boldsymbol{x})} + \underbrace{\left(-\frac{(1 + Z_q)M_\eta}{\tau_\eta}\right)}_{b_3(\boldsymbol{x})} \eta_{\text{cmd}}. \tag{90}$$

The remaining term in Eq. (88) is $\Phi_3(H, \dot{H}, \ddot{H})$, which follows from the HOCBF recursion in Eq. (10). For the present case as was already shown in Eqs.(49) and (50),

$$\begin{aligned} \psi_0 &= H, \\ \psi_1 &= \dot{H} + \gamma_1 H, \\ \psi_2 &= \ddot{H} + (\gamma_1 + \gamma_2)\dot{H} + \gamma_1\gamma_2 H, \end{aligned} \tag{91}$$

and

$$\begin{aligned} \psi_3 &= \dot{\psi}_2 + \gamma_3 \psi_2 \\ &= H^{(3)} + \underbrace{(\gamma_1 + \gamma_2 + \gamma_3)\ddot{H} + (\gamma_1\gamma_2 + \gamma_1\gamma_3 + \gamma_2\gamma_3)\dot{H} + \gamma_1\gamma_2\gamma_3 H}_{\Phi_3(H, \dot{H}, \ddot{H})}. \end{aligned} \tag{92}$$

Thus according to Eq.(108),

$$\Phi_3(H, \dot{H}, \ddot{H}) = (\gamma_1 + \gamma_2 + \gamma_3)\ddot{H} + (\gamma_1\gamma_2 + \gamma_1\gamma_3 + \gamma_2\gamma_3)\dot{H} + \gamma_1\gamma_2\gamma_3 H. \tag{93}$$

7.3.2 OLB Protection Law

Since the present example has relative degree $r = 3$, the OLB limiting input is obtained from Eq. (35) as

$$\eta_{\text{cmd,lim}}^{\text{OLB}} = \frac{1}{\tilde{g}_3}\left[x_{3,d} - \tilde{f}_3\right]. \tag{94}$$

According to the actuator dynamics in Eq. (86),

$$\tilde{f}_3 = -\frac{1}{\tau_\eta}\eta, \qquad \tilde{g}_3 = \frac{1}{\tau_\eta}. \tag{95}$$

The quantity $x_{3,d}$ follows from the recursive OLB law in Eq. (33) with $i = 3$ as

$$x_{3,d} = \frac{1}{g_2}\left[\dot{x}_{2,d} - f_2(x_1, x_2) + g_1 e_1 + c_2 e_2\right]. \tag{96}$$

From the system dynamics in Eq. (35) we obtain the $\ddot{q}$ equation, and $\ddot{\alpha}$ such that we can deduce

$$f_2(x_1, x_2) = M_\alpha \dot{\alpha} + M_q \dot{q}, \qquad g_2 = M_\eta, \qquad g_1 = 1 + Z_q. \tag{97}$$

Furthermore, $e_2 = x_{2,d} - x_2 = x_{2,d} - \dot{q}$. The desired transformed state $x_{2,d}$ is obtained from Eq. (32) as

$$x_{2,d} = \frac{1}{g_1}\left[\dot{\alpha}_{\mathrm{OLB}} - f_1(x_1) + c_1 e_1\right], \tag{98}$$

where

$$f_1(x_1) = Z_\alpha \dot{\alpha}, \qquad g_1 = 1 + Z_q. \tag{99}$$

and with $e_1 = \alpha_{\mathrm{OLB}} - \dot{\alpha} = \gamma_1^{\mathrm{OLB}}(\alpha_{\max} - \alpha) - \dot{\alpha}, \dot{\alpha}_{\mathrm{OLB}} = -\gamma_1^{\mathrm{OLB}}\dot{\alpha}$.

Finally, evaluation of Eq. (96) requires $\dot{x}_{2,d}$. Differentiating Eq. (98) gives

$$\dot{x}_{2,d} = \frac{1}{1 + Z_q}\left[-\left(Z_\alpha + \gamma_1^{\mathrm{OLB}} + c_1\right)\ddot{\alpha} - c_1\gamma_1^{\mathrm{OLB}}\dot{\alpha}\right]. \tag{100}$$

7.4 HOCBF–OLB Limiting-Input Correspondence

The HOCBF and OLB protection laws derived above have different implementations. Nevertheless, for the considered design choices, they lead to the same limiting elevator command if the higher-order correspondence conditions derived in Section 6.2 are satisfied.

Proposition 6 (Limiting-input correspondence for the actuator-augmented short-period model) *Consider the actuator-augmented short-period model in Eq. (86) with the HOCBF and OLB design choices of Section 7.2.*

Let the first HOCBF and OLB gains satisfy

$$\gamma_1^{\mathrm{HOCBF}} = \gamma_1^{\mathrm{OLB}}, \tag{101}$$

and let the remaining gains satisfy

$$\boxed{\gamma_2 + \gamma_3 = c_1 + c_2, \qquad \gamma_2\gamma_3 = c_1 c_2 + (1 + Z_q)^2.} \tag{102}$$

Then the limiting commanded elevator deflections obtained from the respective active HOCBF and OLB protection conditions are identical,

$$\boxed{\eta_{\mathrm{cmd,lim}}^{\mathrm{HOCBF}} = \eta_{\mathrm{cmd,lim}}^{\mathrm{OLB}}.} \tag{103}$$

Proof The proof is given in Appendix E. □

7.5 Simulation Results With Actuator Dynamics

The same reference model and nominal dynamic-inversion controller as in Section 5.5 are used. In particular this means that the nominal controller does not account for the actuator dynamics in Eq. (86). The controller gains, all remaining model, and simulation parameters also remain unchanged.

The same maneuver as in Section 5.6 is considered. Thus, a constant angle-of-attack command of $\alpha_{\mathrm{cmd,raw}} = 15\,\mathrm{deg}$ is applied at $t = 1\,\mathrm{s}$, while the protection limit is $\alpha_{\max} = 10\,\mathrm{deg}$. In contrast to the previous simulation, the first-order actuator dynamics in Eq. (86) are now included in the simulated plant.

Two protection implementations are compared. First, the actuator dynamics are neglected in the protection design. In this case, the relative-degree-two protection laws from Section 5 are applied directly to the actuator-augmented plant. Second, the actuator dynamics are explicitly included in the protection design using the relative-degree-three laws derived in Sections 7.3.1 and 7.3.2. The HOCBF and OLB parameters are matched according to the corresponding analytical correspondence conditions.

The main objective of these simulations is to verify the analytically derived equivalence between HOCBF and OLB for relative degree three. The results confirm that both approaches yield identical limiting control inputs when the design parameters satisfy the correspondence conditions in Proposition 6. This extends the numerical demonstration of equivalence from relative degree two in Section 5.6 to a higher-order system with additional recursive steps.

Figure 7 compares the resulting responses. For a more conservative phase-plane boundary, i.e. low γ_1 value, neglecting the actuator dynamics has only a small influence on the protection performance. The additional actuator dynamics can therefore be neglected in this case.

The difference becomes significant for a more aggressive protection design depicted in Fig. 8. A larger value of γ_1 permits a faster approach toward the angle-of-attack limit and therefore requires faster control action when close to the limit. If the actuator dynamics are neglected in the protection law, the commanded control action cannot be realized sufficiently fast by the actuator. This can lead to strongly degraded behavior and, for sufficiently aggressive settings, instability or oscillations. In contrast, explicitly including the actuator dynamics in the protection design accounts for this additional dynamic limitation and provides improved protection performance.

These results illustrate that neglecting sufficiently fast actuator dynamics can be acceptable for conservative protection designs. However, explicitly accounting for the actuator dynamics becomes increasingly important when the protection boundary is chosen aggressively in order to reduce conservatism.

However, it shall be kept in mind that a drawback of the higher-order formulation is the increased amount of state information required for its implementation. For example, evaluation of the protection laws in Eqs. (88) and (100) requires quantities such as $\dot{\alpha}$, $\ddot{\alpha}$, and $\dot{q}$. These quantities may not be directly available from measurements and must in practice be obtained from suitable measurements, models, or estimations

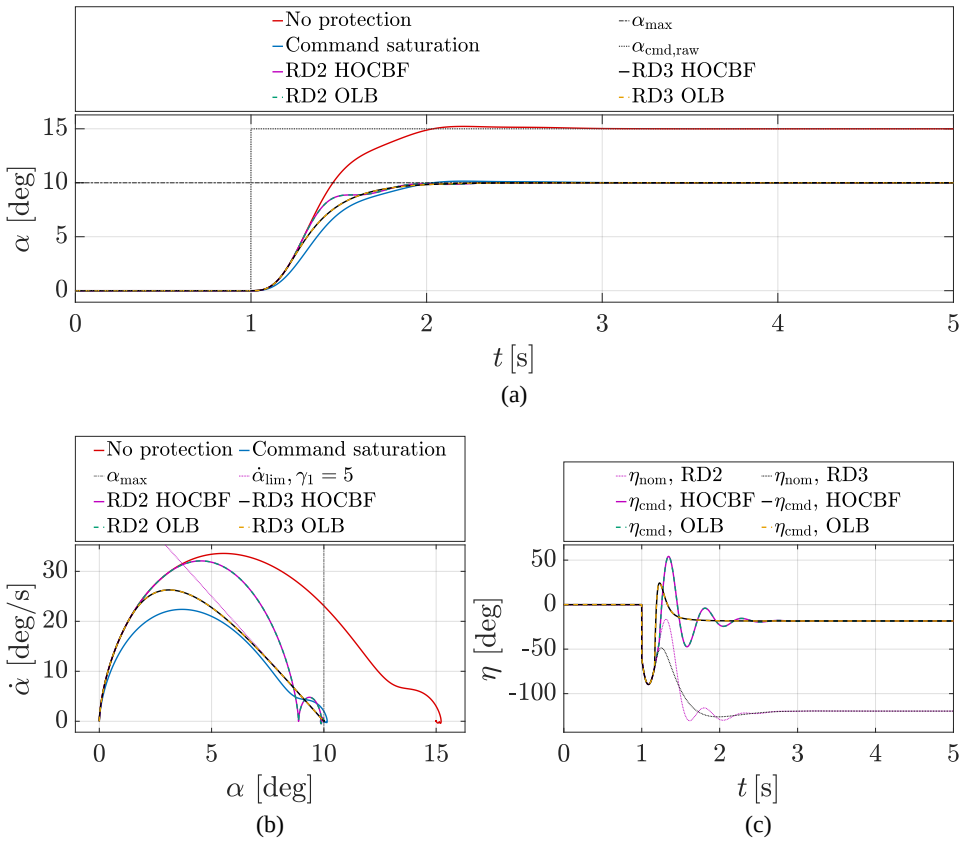


Fig. 7: Simulation results with actuator dynamics for a non-aggressive protection design.

and might introduce an increased level of measurement noise. The design of such estimation schemes is outside the scope of this paper.

8 Conclusion

This work compared Output Limiting with Backstepping (OLB) and Higher-Order Control Barrier Functions (HOCBFs) for output protection. We established a mathematical relationship between the two approaches and identified conditions under which they lead to identical limiting control laws. This was also demonstrated in simulations of an aircraft short-period model, both with and without actuator dynamics.

The results show that phase-plane limits used in OLB can provide a useful interpretation of HOCBF design parameters. Future work could investigate how the derived relationship can be used to design HOCBFs based on nonlinear or piecewise-polynomial phase-plane boundaries, and assess the feasibility and practical benefits of such an approach.

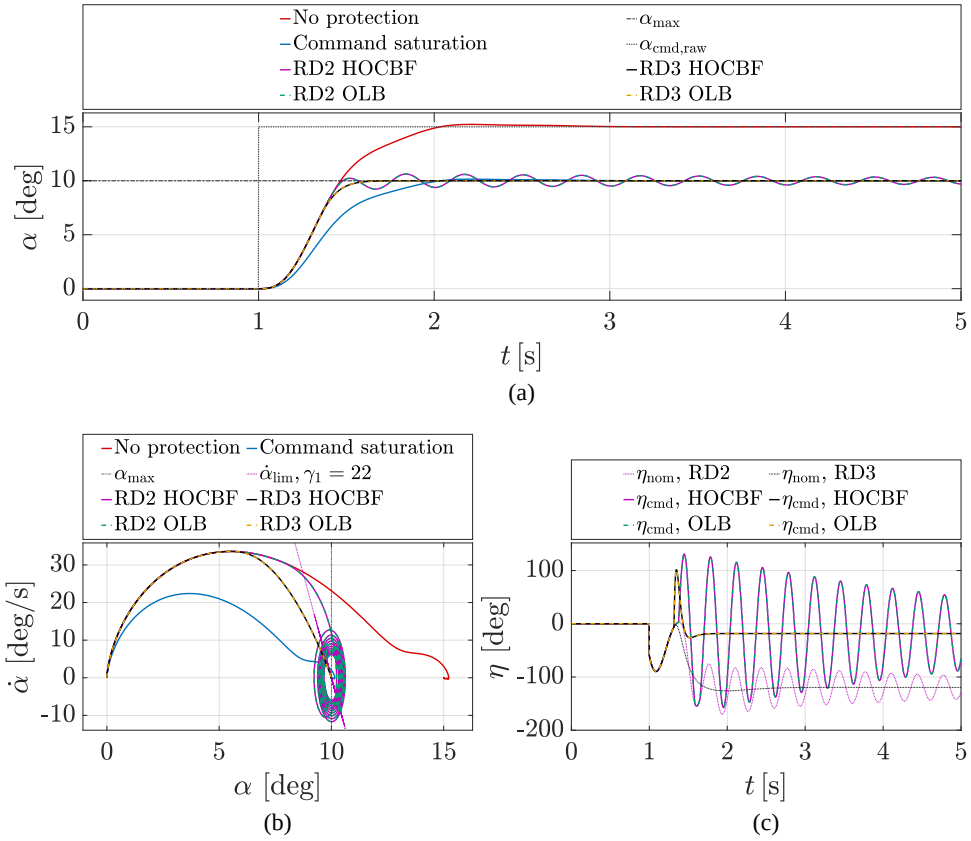


Fig. 8: Simulation results with actuator dynamics.

The simulations further indicate that neglecting actuator dynamics in the protection design can lead to oscillations or instability when aggressive protection parameters are chosen. Future work could therefore investigate under which conditions actuator dynamics need to be considered explicitly in the protection design. This could also be extended to systems with multiple actuators with different dynamics, including the effects of neglecting these dynamics and the resulting interactions.

A Mathematical Details of the HOCBF Construction

This appendix collects the mathematical details underlying the HOCBF recursion in Eq. (10).

A.1 Class-$\mathcal{K}$ Functions and Regularity Requirements

Definition 5 (Class-$\mathcal{K}$ Function) A class-$\mathcal{K}$ function α is continuous and strictly increasing, that is, for any

$$s_1 < s_2 \quad \Longrightarrow \quad \alpha(s_1) < \alpha(s_2). \tag{104}$$

Furthermore, it satisfies

$$\alpha(0) = 0. \tag{105}$$

Assumption 1 (Regularity of the Class-$\mathcal{K}$ Functions) For an HOCBF recursion of relative degree r, the class-$\mathcal{K}$ functions α_i are chosen such that

$$\alpha_i \in C^{r-i}, \qquad i = 1, \dots, r. \tag{106}$$

The required differentiability follows from the recursive construction. In the HOCBF recursion, the functions α_i are repeatedly differentiated. The required differentiability becomes visible from the first two recursive quantities. Using the recursion in Eq. (10) gives

$$\begin{aligned} \psi_1 &= \dot{\psi}_0 + \alpha_1(\psi_0) = \dot{H} + \alpha_1(H), \\ \psi_2 &= \dot{\psi}_1 + \alpha_2(\psi_1) = \ddot{H} + \dot{\alpha}_1(H) + \alpha_2(\psi_1) = \ddot{H} + \frac{\partial \alpha_1(H)}{\partial H}\dot{H} + \alpha_2(\psi_1). \end{aligned} \tag{107}$$

Thus, construction of ψ_2 already requires one derivative of α_1. Continuing the recursion up to r differentiates α_1 up to $r-1$ times, α_2 up to $r-2$ times, and in general, α_i up to $r-i$ times.

A.2 Appearance of the Control Input in the HOCBF Recursion

Lemma 7 (Appearance of the Control Input in the HOCBF Recursion) *Let $H(\boldsymbol{x})$ have relative degree r, and let the recursive quantities ψ_i be defined by Eq. (10). Then the physical control input $\boldsymbol{u}$ does not appear explicitly in $\psi_0, \dots, \psi_{r-1}$ and appears for the first time in ψ_r.*

Proof Equation (107) shows that every recursive step introduces one additional derivative of H, while the differentiated class-$\mathcal{K}$ functions generate terms containing lower-order derivatives of H. Repeating the recursion therefore gives

$$\psi_i = H^{(i)} + \Phi_i\left(H, \dot{H}, \dots, H^{(i-1)}\right), \qquad i = 1, \dots, r, \tag{108}$$

where Φ_i collects the terms generated by the class-$\mathcal{K}$ functions and their derivatives. Substituting the relative-degree relation in Eq. (9),

$$H^{(r)} = a_r(\boldsymbol{x}) + b_r(\boldsymbol{x})\boldsymbol{u}, \qquad b_r(\boldsymbol{x}) \neq 0. \tag{109}$$

into Eq. (108), for $i = r$, gives

$$\psi_r = a_r(\boldsymbol{x}) + b_r(\boldsymbol{x})\boldsymbol{u} + \Phi_r\left(H, \dot{H}, \dots, H^{(r-1)}\right), \tag{110}$$

so that $\boldsymbol{u}$ appears explicitly for the first time in ψ_r. □

A.3 Recursive HOCBF Sets

Definition 6 (Recursive HOCBF Sets) For each recursive quantity ψ_{i-1} defined in Eq. (10), define the corresponding state set as

$$\begin{aligned} C_1 &= \{\boldsymbol{x} \mid \psi_0(\boldsymbol{x}) \geq 0\}, \qquad C_2 = \{\boldsymbol{x} \mid \psi_1(\boldsymbol{x}) \geq 0\}, \\ &\dots, \qquad C_r = \{\boldsymbol{x} \mid \psi_{r-1}(\boldsymbol{x}) \geq 0\}. \end{aligned} \tag{111}$$

Using $\psi_0 = H(\boldsymbol{x})$ from Eq. (10) gives

$$C_1 = \{\boldsymbol{x} \mid H(\boldsymbol{x}) \geq 0\} = \mathcal{X}_{\text{safe}}. \tag{112}$$

Thus, C_1 is the original safe state set. The sets $C_2, \ldots, C_r$ analogously contain the states for which the corresponding higher-order recursive quantities are nonnegative. These are definitions of the sets; whether a trajectory remains in them is established by the forward-invariance proof in Appendix A.5.

A.4 Forward Invariance

Definition 7 (Forward Invariance) A set C is forward invariant if

$$\boldsymbol{x}(t_0) \in C \quad \Longrightarrow \quad \boldsymbol{x}(t) \in C, \qquad \forall\, t \geq t_0, \tag{113}$$

for all times for which the solution exists.

For the first recursive set $C_1 = \mathcal{X}_{\text{safe}}$, forward invariance therefore means that a trajectory starting with $H(\boldsymbol{x}(t_0)) \geq 0$ satisfies $H(\boldsymbol{x}(t)) \geq 0$, and hence $y(t) \leq y_{\max}$, for all subsequent times.

A.5 Proof of the HOCBF Forward-Invariance Result

Proof of Theorem 1 Using the HOCBF condition in Eq. (11) and the recursive definition in Eq. (10) gives

$$\psi_r = \dot{\psi}_{r-1} + \alpha_r(\psi_{r-1}) \geq 0, \tag{114}$$

and therefore

$$\dot{\psi}_{r-1} \geq -\alpha_r(\psi_{r-1}). \tag{115}$$

From the class-$\mathcal{K}$ properties in Definition 5, $\alpha_r(0) = 0$. Since α_r is strictly increasing, $0 < \xi$ implies $\alpha_r(0) < \alpha_r(\xi)$, and therefore $\alpha_r(\xi) > 0$.

In particular, at the boundary $\psi_{r-1} = 0$, Eq. (115) gives

$$\dot{\psi}_{r-1} \geq -\alpha_r(0) = 0. \tag{116}$$

At this boundary, the rate of ψ_{r-1} is therefore nonnegative. Hence, ψ_{r-1} cannot decrease through zero toward negative values. Together with the initial condition $\psi_{r-1}(\boldsymbol{x}(t_0)) \geq 0$, this gives

$$\psi_{r-1}(\boldsymbol{x}(t)) \geq 0, \qquad \forall\, t \geq t_0. \tag{117}$$

Thus, the trajectory remains in C_r defined in Definition 6.

Using the recursive definition in Eq. (10) for $i = r - 1$ then gives

$$\psi_{r-1} = \dot{\psi}_{r-2} + \alpha_{r-1}(\psi_{r-2}) \geq 0. \tag{118}$$

Applying the same argument together with the initial condition $\psi_{r-2}(\boldsymbol{x}(t_0)) \geq 0$ gives $\psi_{r-2}(\boldsymbol{x}(t)) \geq 0$. Repeating the argument recursively yields

$$\psi_{r-1} \geq 0 \implies \psi_{r-2} \geq 0 \implies \cdots \implies \psi_0 = H \geq 0. \tag{119}$$

Consequently,

$$\boldsymbol{x}(t) \in C_1 \cap C_2 \cap \cdots \cap C_r, \qquad \forall\, t \geq t_0. \tag{120}$$

Hence, the intersection $C_1 \cap C_2 \cap \cdots \cap C_r$ is forward invariant according to Definition 7. Since $C_1 = \mathcal{X}_{\text{safe}}$ from Eq. (112), the trajectory also remains in the safe state set and consequently

$$H(\boldsymbol{x}(t)) \geq 0 \quad \Longleftrightarrow \quad y(t) \leq y_{\max}, \tag{121}$$

which proves the output-safety result. □

B Mathematical Details of the OLB Construction

This appendix collects the mathematical details underlying the OLB construction introduced in Section 4.

B.1 Derivation of the Transformed System

This subsection derives the transformed system used to formulate the tracking problem and backstepping limiting law. Starting from the physical triangular system in Eq. (23), consider the i-th subsystem,

$$\dot{\tilde{x}}_i = \tilde{f}_i(\tilde{x}_1, \ldots, \tilde{x}_i) + \tilde{g}_i \tilde{x}_{i+1}, \qquad i = 1, \ldots, r-1. \tag{122}$$

The transformed states are defined in Eq. (26) as $x_i = \dot{\tilde{x}}_i$. Differentiating Eq. (122) and substituting this transformation gives

$$\begin{aligned} \dot{x}_i &= \ddot{\tilde{x}}_i \\ &= \sum_{j=1}^{i} \frac{\partial \tilde{f}_i}{\partial \tilde{x}_j} \dot{\tilde{x}}_j + \tilde{g}_i \dot{\tilde{x}}_{i+1} \\ &= \underbrace{\sum_{j=1}^{i} \frac{\partial \tilde{f}_i}{\partial \tilde{x}_j} x_j}_{f_i(\tilde{x}_1, \ldots, \tilde{x}_i, x_1, \ldots, x_i)} + \underbrace{\tilde{g}_i}_{g_i} x_{i+1}, \qquad i = 1, \ldots, r-1. \end{aligned} \tag{123}$$

Thus, differentiation preserves the triangular connection between the transformed states. In general, however, the functions f_i still depend on the physical states $\tilde{\boldsymbol{x}}$.

If the OLB system class considered, is further restricted to systems for which

$$\frac{\partial \tilde{f}_i}{\partial \tilde{x}_j} = a_{ij} = \text{const.}, \qquad j = 1, \ldots, i. \tag{124}$$

then substituting Eq. (124) into Eq. (123) gives

$$\begin{aligned} \dot{x}_i &= f_i(x_1, \ldots, x_i) + g_i x_{i+1}, \qquad i = 1, \ldots, r-1, \\ f_i(x_1, \ldots, x_i) &= \sum_{j=1}^{i} a_{ij} x_j, \qquad g_i = \tilde{g}_i. \end{aligned} \tag{125}$$

Hence, the transformed dynamics have the triangular form

$$\begin{aligned} \dot{x}_1 &= f_1(x_1) + g_1 x_2, \\ \dot{x}_2 &= f_2(x_1, x_2) + g_2 x_3, \\ &\vdots \\ \dot{x}_{r-1} &= f_{r-1}(x_1, \ldots, x_{r-1}) + g_{r-1} x_r. \end{aligned} \tag{126}$$

For this system representation classical recursive backstepping design can be applied straight forward.

B.2 Proof of the Recursive OLB Law

Proof of Proposition 2 **First recursive step.** The first tracking error is

$$e_1 = \alpha_{\mathrm{OLB}}(y, y_{\max}) - x_1. \tag{127}$$

To determine the desired value of x_2, consider the quadratic Lyapunov function

$$V_1 = \frac{1}{2} e_1^2. \tag{128}$$

The virtual control $x_{2,d}$ is chosen such that the derivative of V_1 is negative definite if $x_2 = x_{2,d}$.

Differentiating the tracking error in Eq. (127) and substituting the first transformed state derivative $\dot{x}_1 = f_1(x_1) + g_1 x_2$ from Eq. (126) gives

$$\dot{e}_1 = \dot{\alpha}_{\mathrm{OLB}} - f_1(x_1) - g_1 x_2. \tag{129}$$

Differentiating the Lyapunov function in Eq. (128), substituting the error derivative from Eq. (129), and requiring a negative-definite derivative for $x_2 = x_{2,d}$ gives

$$\dot{V}_1 = e_1 \left[\dot{\alpha}_{\mathrm{OLB}} - f_1(x_1) - g_1 x_{2,d}\right] \stackrel{!}{=} -c_1 e_1^2, \qquad c_1 > 0. \tag{130}$$

Solving Eq. (130) for $x_{2,d}$ gives

$$x_{2,d} = \frac{1}{g_1} \left[\dot{\alpha}_{\mathrm{OLB}} - f_1(x_1) + c_1 e_1\right]. \tag{131}$$

Thus, if $x_2 = x_{2,d}$, the desired Lyapunov derivative in Eq. (130) is obtained. However, x_2 cannot be assigned directly. Therefore, define the next tracking error as

$$e_2 = x_{2,d} - x_2, \qquad x_2 = x_{2,d} - e_2. \tag{132}$$

Substituting Eq. (132) and the desired value $x_{2,d}$ from Eq. (131) into the Lyapunov derivative in Eq. (130) gives

$$\dot{V}_1 = -c_1 e_1^2 + g_1 e_1 e_2. \tag{133}$$

The next backstepping step must therefore drive e_2 toward zero while cancelling the remaining cross term $g_1 e_1 e_2$.

General recursive step.

For $i = 2, \ldots, r-1$, define

$$e_i = x_{i,d} - x_i \tag{134}$$

and extend the Lyapunov function recursively as

$$V_i = V_{i-1} + \frac{1}{2} e_i^2 = \frac{1}{2} \sum_{j=1}^{i} e_j^2. \tag{135}$$

After the preceding backstepping step,

$$\dot{V}_{i-1} = -\sum_{j=1}^{i-1} c_j e_j^2 + g_{i-1} e_{i-1} e_i. \tag{136}$$

Equation (133) is the first instance of this structure.

The next desired state $x_{i+1,d}$ is chosen such that, for $x_{i+1} = x_{i+1,d}$, the Lyapunov function satisfies

$$\dot{V}_i \stackrel{!}{=} -\sum_{j=1}^{i} c_j e_j^2. \tag{137}$$

Differentiating the error e_i from Eq. (134) and substituting the i-th transformed state derivative $\dot{x}_i = f_i(x_1, \ldots, x_i) + g_i x_{i+1}$ from Eq. (126) gives

$$\dot{e}_i = \dot{x}_{i,d} - f_i(x_1, \ldots, x_i) - g_i x_{i+1}. \tag{138}$$

Differentiating the Lyapunov function in Eq. (135), and substituting the preceding derivative $\dot{V}_{i-1}$ from Eq. (136) and the error dynamics from Eq. (138), gives

$$\begin{aligned} \dot{V}_i &= \dot{V}_{i-1} + e_i \dot{e}_i \\ &= -\sum_{j=1}^{i-1} c_j e_j^2 + e_i \left[g_{i-1} e_{i-1} + \dot{x}_{i,d} - f_i(x_1, \ldots, x_i) - g_i x_{i+1} \right]. \end{aligned} \tag{139}$$

Comparing the actual derivative in Eq. (139) with the desired derivative in Eq. (137), the desired state $x_{i+1,d}$ must satisfy

$$g_{i-1} e_{i-1} + \dot{x}_{i,d} - f_i(x_1, \ldots, x_i) - g_i x_{i+1,d} = -c_i e_i. \tag{140}$$

Solving for $x_{i+1,d}$ gives

$$x_{i+1,d} = \frac{1}{g_i} \left[\dot{x}_{i,d} - f_i(x_1, \ldots, x_i) + g_{i-1} e_{i-1} + c_i e_i \right]. \tag{141}$$

If $x_{i+1} = x_{i+1,d}$, Eq. (141) gives exactly the desired Lyapunov derivative in Eq. (137). Since x_{i+1} is again not directly assignable before the final step, define

$$e_{i+1} = x_{i+1,d} - x_{i+1}. \tag{142}$$

Substituting $x_{i+1} = x_{i+1,d} - e_{i+1}$ and the desired value in Eq. (141) into Eq. (139) gives

$$\dot{V}_i = -\sum_{j=1}^{i} c_j e_j^2 + g_i e_i e_{i+1}. \tag{143}$$

Equation (143) has the same structure as Eq. (136). The construction can therefore be repeated recursively until the final desired transformed state $x_{r,d}$ is obtained.

□

C Proof of the HOCBF-OLB Correspondence

This appendix proves the three statements of Proposition 3 separately.

C.1 Phase-Plane and Recursive-Quantity Correspondence

Proof of Proposition 3, Statement 1 For OLB, substituting the phase-plane limit in Eq. (42) into the tracking-error definition in Eq. (43) gives

$$e_1 = \dot{\alpha}_{lim} - \dot{\alpha} = \gamma_1^{\mathrm{OLB}}(\alpha_{\max} - \alpha) - \dot{\alpha}. \tag{144}$$

For HOCBF, substituting into the recursion from Eq. (10),

$$\psi_1 = \dot{\psi}_0 + \alpha_1(\psi_0), \tag{145}$$

the safety function $H(\alpha) = \alpha_{\max} - \alpha = \Psi_0$ in Eq. (44) and the first class-$\mathcal{K}$ function α_1 in Eq. (45) gives

$$\psi_1 = -\dot{\alpha} + \gamma_1^{\text{HOCBF}}(\alpha_{\max} - \alpha). \tag{146}$$

Comparing Eqs. (144) and (146) gives

$$\boxed{\psi_1 = e_1.} \tag{147}$$

if the gains are chosen according to Eq. (55), i.e. $\gamma_1^{\text{HOCBF}} = \gamma_1^{\text{OLB}}$.

With the HOCBF condition $\psi_1 \geq 0$, Eq. (146) is then equivalent to

$$\boxed{\dot{\alpha} \leq \gamma_1^{\text{HOCBF}}(\alpha_{\max} - \alpha) = \gamma_1^{\text{OLB}}(\alpha_{\max} - \alpha) = \dot{\alpha}_{\text{lim}},} \tag{148}$$

which is exactly the OLB phase-plane limit in Eq. (42). On its boundary, $\dot{\alpha} = \dot{\alpha}_{\text{lim}}$. This proves Statement 1. □

C.2 Active Error-Dynamics Correspondence

Proof of Proposition 3, Statement 2 For the relative-degree-two HOCBF, the recursion in Eq. (10) gives

$$\psi_2 = \dot{\psi}_1 + \alpha_2(\psi_1). \tag{149}$$

On the active boundary of the HOCBF control constraint, $\psi_2 = 0$. Substituting $\alpha_2(\psi_1) = \gamma_2\psi_1$ from Eq. (45) into Eq. (149) therefore gives

$$\boxed{\dot{\psi}_1 = -\gamma_2\psi_1.} \tag{150}$$

For OLB, the transformed states are $x_1 = \dot{\alpha}, x_2 = \dot{q}$. Using Eq. (38), their first transformed subsystem is

$$\dot{x}_1 = Z_\alpha x_1 + (1 + Z_q)x_2. \tag{151}$$

Thus,

$$f_1(x_1) = Z_\alpha x_1, \qquad g_1 = 1 + Z_q. \tag{152}$$

Differentiating the OLB error $e_1 = \dot{\alpha}_{\text{lim}} - \dot{\alpha}$ in Eq. (43) and using the transformed subsystem in Eq. (151) gives

$$\dot{e}_1 = \dot{\alpha}_{\text{OLB}} - f_1(x_1) - g_1 x_2, \tag{153}$$

where $\dot{\alpha}_{\text{OLB}}$ denotes the time derivative of the phase-plane function $\dot{\alpha}_{\text{lim}} = \alpha_{\text{OLB}}(\alpha, \alpha_{\max})$. The first desired transformed state of the OLB recursion is given by Eq. (32),

$$x_{2,d} = \frac{1}{g_1}\left[\dot{\alpha}_{\text{OLB}} - f_1(x_1) + c_1 e_1\right]. \tag{154}$$

During active limiting, $x_2 = x_{2,d}$. Substituting Eq. (154) into the error dynamics in Eq. (153) gives

$$\dot{e}_1 = \dot{\alpha}_{\text{OLB}} - f_1(x_1) - \left[\dot{\alpha}_{\text{OLB}} - f_1(x_1) + c_1 e_1\right] \tag{155}$$

Hence,

$$\boxed{\dot{e}_1 = -c_1 e_1.} \tag{156}$$

If $\gamma_1^{\text{HOCBF}} = \gamma_1^{\text{OLB}}$ then $\psi_1 = e_1$ according to Eq. (56). If additionally

$$\boxed{c_1 = \gamma_2,} \tag{157}$$

is imposed, then comparison of Eqs. (150) and (156) shows that the active error dynamics are identical.

This proves Statement 2. □

C.3 Limiting-Control Correspondence

Proof of Proposition 3, Statement 3 For HOCBF, substituting the functions $H = \alpha_{\max} - \alpha$, $\alpha_1(H) = \gamma_1^{\text{HOCBF}} H$, and $\alpha_2(\psi_1) = \gamma_2 \psi_1$ from Eqs. (44) and (45) into the second recursion in Eq. (149) gives

$$\begin{aligned}\psi_2 &= \dot{\psi}_1 + \alpha_2(\psi_1) = \ddot{H} + \frac{\mathrm{d}\alpha_1}{\mathrm{d}H}\dot{H} + \alpha_2(\psi_1) \\ &= -\ddot{\alpha} - \gamma_1^{\text{HOCBF}}\dot{\alpha} + \gamma_2\left[-\dot{\alpha} + \gamma_1^{\text{HOCBF}}(\alpha_{\max} - \alpha)\right] \\ &= -\ddot{\alpha} - \left(\gamma_1^{\text{HOCBF}} + \gamma_2\right)\dot{\alpha} + \gamma_1^{\text{HOCBF}}\gamma_2(\alpha_{\max} - \alpha).\end{aligned} \tag{158}$$

The limiting HOCBF input lies on the active boundary $\psi_2 = 0$. Substituting the angle-of-attack dynamics $\ddot{\alpha}$ from Eq. (38) into Eq. (158) and setting $\psi_2 = 0$ gives

$$\begin{aligned}0 = &-Z_\alpha\dot{\alpha} - (1+Z_q)\left(M_\alpha\alpha + M_q q + M_\eta\eta\right) \\ &- \left(\gamma_1^{\text{HOCBF}} + \gamma_2\right)\dot{\alpha} + \gamma_1^{\text{HOCBF}}\gamma_2(\alpha_{\max} - \alpha).\end{aligned} \tag{159}$$

Solving Eq. (159) for the elevator input gives

$$\boxed{\eta_{\text{lim}}^{\text{HOCBF}} = \frac{-\left(Z_\alpha + \gamma_1^{\text{HOCBF}} + \gamma_2\right)\dot{\alpha} - (1+Z_q)(M_\alpha\alpha + M_q q) + \gamma_1^{\text{HOCBF}}\gamma_2(\alpha_{\max} - \alpha)}{(1+Z_q)M_\eta}.} \tag{160}$$

For OLB, differentiating the phase-plane function in Eq. (42) gives

$$\dot{\alpha}_{\text{OLB}} = \frac{\mathrm{d}}{\mathrm{d}t}\left[\gamma_1(\alpha_{\max} - \alpha)\right] = -\gamma_1^{\text{OLB}}\dot{\alpha}. \tag{161}$$

Substituting Eq. (161), $x_1 = \dot{\alpha}$, the quantities $f_1(x_1) = Z_\alpha x_1, g_1 = 1 + Z_q$ from Eq. (152), and the OLB error from Eq. (144) into the desired transformed state in Eq. (154) gives

$$\begin{aligned}x_{2,d} &= \frac{1}{g_1}\left[\dot{\alpha}_{\text{OLB}} - f_1(x_1) + c_1 e_1\right] \\ &= \frac{1}{1+Z_q}\left[-\gamma_1^{\text{OLB}}\dot{\alpha} - Z_\alpha\dot{\alpha} + c_1\left(\gamma_1^{\text{OLB}}(\alpha_{\max} - \alpha) - \dot{\alpha}\right)\right] \\ &= \frac{-\left(Z_\alpha + \gamma_1^{\text{OLB}} + c_1\right)\dot{\alpha} + c_1\gamma_1^{\text{OLB}}(\alpha_{\max} - \alpha)}{1+Z_q}.\end{aligned} \tag{162}$$

The second aircraft equation in Eq. (36) is,

$$x_2 = \dot{q} = M_\alpha\alpha + M_q q + M_\eta\eta. \tag{163}$$

During active limiting, $x_2 = x_{2,d}$. Substituting Eq. (162) into Eq. (163) and solving for η gives

$$\boxed{\eta_{\text{lim}}^{\text{OLB}} = \frac{-\left(Z_\alpha + \gamma_1^{\text{OLB}} + c_1\right)\dot{\alpha} - (1+Z_q)(M_\alpha\alpha + M_q q) + c_1\gamma_1^{\text{OLB}}(\alpha_{\max} - \alpha)}{(1+Z_q)M_\eta}.} \tag{164}$$

Equations (160) and (164) show the two matching requirements directly. Applying

$$\gamma_1^{\text{OLB}} = \gamma_1^{\text{HOCBF}}, \qquad c_1 = \gamma_2 \tag{165}$$

leads to

$$\boxed{\eta_{\text{lim}}^{\text{HOCBF}} = \eta_{\text{lim}}^{\text{OLB}}.} \tag{166}$$

This proves Statement 3. □

D Proofs of the General HOCBF–OLB Correspondence

D.1 Proof of the First-Level Correspondence

Proof of Proposition 4 For OLB, the physical phase-plane boundary is defined in Eq. (19) as

$$\dot{y}_{\lim}^{\mathrm{OLB}} = \alpha_{\mathrm{OLB}}(y, y_{\max}). \tag{167}$$

For HOCBF, Eq. (10) with $i = 1$ gives $\psi_1 = \dot{\psi}_0 + \alpha_1(\psi_0)$ with $\psi_0 = H$. Moreover, $H(\boldsymbol{x}) = h(y = p(\boldsymbol{x}))$. Hence, $\dot{H} = (\partial h/\partial y)\dot{y}$. Substituting these relations into the first HOCBF recursion, applying $\psi_1 \geq 0$, and using $\partial h/\partial y < 0$ gives

$$\begin{aligned} \psi_1 &= \dot{\psi}_0 + \alpha_1(\psi_0) = \dot{H} + \alpha_1(H) \\ &= \frac{\partial h}{\partial y}\dot{y} + \alpha_1(h(y)) \geq 0 \\ \iff \qquad & \dot{y} \leq \frac{\alpha_1(h(y))}{-\frac{\partial h}{\partial y}} = \dot{y}_{\lim}^{\mathrm{HOCBF}}. \end{aligned} \tag{168}$$

Comparing the HOCBF phase-plane boundary in Eq. (168) with the OLB boundary in Eq. (167) gives

$$\boxed{\alpha_1(h(y)) = -\frac{\partial h}{\partial y}\alpha_{\mathrm{OLB}}(y, y_{\max}),} \tag{169}$$

which proves the phase-plane correspondence in Eq. (70).

Substituting into the first HOCBF quantity ψ_1 given in Eq. (168), the α_1 from Eq. (169), and using the OLB tracking-error definition $e_1 = \alpha_{\mathrm{OLB}}(y, y_{\max}) - \dot{y}$ in Eq. (27) gives

$$\psi_1 = \frac{\partial h}{\partial y}\dot{y} - \frac{\partial h}{\partial y}\alpha_{\mathrm{OLB}}(y, y_{\max}) = -\frac{\partial h}{\partial y}\left(\alpha_{\mathrm{OLB}}(y, y_{\max}) - \dot{y}\right) \tag{170}$$

and hence

$$\boxed{\psi_1 = -\frac{\partial h}{\partial y}e_1} \tag{171}$$

For the affine safety function $h(y) = k(y_{\max} - y)$ from Eq. (73), $\partial h/\partial y = -k$. Substituting this relation into Eq. (171) gives

$$\psi_1 = k\, e_1, \tag{172}$$

which completes the proof. □

D.2 Proofs of the Higher-Order Correspondence

For convenience note that for the safety function in Eq. (77), Eq. (78) gives

$$\psi_1 = ce_1, \qquad \dot{\psi}_1 = c\dot{e}_1, \qquad c > 0. \tag{173}$$

D.2.1 One OLB Backstepping Recursion

Proof of Proposition 5, Statement (ii)(a) Using the HOCBF recursion in Eq. (10) for $i = 2$, together with the linear class-$\mathcal{K}$ function $\alpha_2(\psi_1) = \gamma_2\psi_1$ from Eq. (79), gives $\psi_2 = \dot{\psi}_1 + \gamma_2\psi_1$. Substituting Eq. (173) and imposing the active HOCBF boundary $\psi_2 = 0$ gives

$$\begin{aligned} 0 &= \dot{\psi}_1 + \gamma_2\psi_1 \\ &= c\dot{e}_1 + \gamma_2 ce_1 \\ &= c\left(\dot{e}_1 + \gamma_2 e_1\right). \end{aligned} \tag{174}$$

Since $c > 0$,

$$\dot{e}_1 = -\gamma_2 e_1. \tag{175}$$

For OLB, the desired first-error dynamics $\dot{e}_1 = -c_1 e_1$ follow from $x_2 = x_{2,d}$ by substituting $x_{2,d}$ given in Eq. (131) into the $\dot{e}_1$ equation in Eq. (129). Comparing $\dot{e}_1 = -c_1 e_1$ with Eq. (175) shows that both active error dynamics coincide if $\gamma_2 = c_1$. This proves Statement (ii)(a). □

D.2.2 Two OLB Backstepping Recursions

Proof of Proposition 5, Statement (ii)(b) For HOCBF, using the recursion in Eq. (10) for $i = 2$ and $i = 3$, together with the linear class-$\mathcal{K}$ functions in Eq. (82), gives

$$\psi_2 = \dot{\psi}_1 + \gamma_2 \psi_1, \qquad \psi_3 = \dot{\psi}_2 + \gamma_3 \psi_2.$$

Substituting $\psi_1 = ce_1$ and $\dot{\psi}_1 = c\dot{e}_1$ from Eq. (173) first into ψ_2, and then substituting the resulting expression for ψ_2 into ψ_3, gives

$$\begin{aligned} \psi_2 &= c\dot{e}_1 + \gamma_2 c e_1 \\ &= c\left(\dot{e}_1 + \gamma_2 e_1\right), \\ \psi_3 &= \frac{\mathrm{d}}{\mathrm{d}t}\left[c\left(\dot{e}_1 + \gamma_2 e_1\right)\right] + \gamma_3 c\left(\dot{e}_1 + \gamma_2 e_1\right) \\ &= c\left[\ddot{e}_1 + (\gamma_2 + \gamma_3)\dot{e}_1 + \gamma_2\gamma_3 e_1\right]. \end{aligned} \tag{176}$$

Imposing the active boundary condition $\psi_3 = 0$ and using $c > 0$, the active HOCBF error dynamics are

$$\boxed{\ddot{e}_1 + (\gamma_2 + \gamma_3)\dot{e}_1 + \gamma_2\gamma_3 e_1 = 0.} \tag{177}$$

For OLB, the first tracking error is defined in Eq. (28) as $e_1 = x_{1,d} - x_1$. Differentiating and using the first transformed state derivative $\dot{x}_1 = f_1(x_1) + g_1 x_2$ gives

$$\dot{e}_1 = \dot{x}_{1,d} - f_1(x_1) - g_1 x_2. \tag{178}$$

The first desired transformed state is given in Eq. (32) by

$$x_{2,d} = \frac{1}{g_1}\left[\dot{x}_{1,d} - f_1(x_1) + c_1 e_1\right]. \tag{179}$$

with $\alpha_{\mathrm{OLB}}(y, y_{\max}) = \dot{x}_{1,d} = \dot{y}_{\lim}$ Using the tracking-error relation $e_2 = x_{2,d} - x_2$, or equivalently $x_2 = x_{2,d} - e_2$, in Eq. (178) and substituting Eq. (179) gives

$$\begin{aligned} \dot{e}_1 &= \dot{x}_{1,d} - f_1(x_1) - g_1\left(x_{2,d} - e_2\right) \\ &= -c_1 e_1 + g_1 e_2. \end{aligned} \tag{180}$$

For the second tracking error, using that at the final active limiting step, $x_3 = x_{3,d}$ with $x_{3,d}$ defined in the recursive OLB law in Eq. (33) as

$$x_{3,d} = \frac{1}{g_2}\left[\dot{x}_{2,d} - f_2(x_1, x_2) + g_1 e_1 + c_2 e_2\right]. \tag{181}$$

gives

$$\begin{aligned} \dot{e}_2 &= \dot{x}_{2,d} - f_2(x_1, x_2) - g_2 x_{3,d} \\ &= -g_1 e_1 - c_2 e_2. \end{aligned} \tag{182}$$

Hence, the corresponding two-step active OLB error dynamics are

$$\dot{e}_1 = -c_1 e_1 + g_1 e_2, \qquad \dot{e}_2 = -g_1 e_1 - c_2 e_2. \tag{183}$$

Differentiating $\dot{e}_1$ in Eq. (183), substituting $\dot{e}_2$, and using $g_1 e_2 = \dot{e}_1 + c_1 e_1$ from the first relation gives

$$\begin{aligned} \ddot{e}_1 &= -c_1 \dot{e}_1 + g_1 \dot{e}_2 \\ &= -c_1 \dot{e}_1 - g_1^2 e_1 - c_2 g_1 e_2 \\ &= -(c_1 + c_2)\dot{e}_1 - (c_1 c_2 + g_1^2) e_1. \end{aligned} \tag{184}$$

Hence,

$$\boxed{\ddot{e}_1 + (c_1 + c_2)\dot{e}_1 + (c_1 c_2 + g_1^2) e_1 = 0.} \tag{185}$$

Comparing Eqs. (177) and (185), the active HOCBF and OLB error dynamics are identical if

$$\boxed{\begin{aligned} \gamma_2 + \gamma_3 &= c_1 + c_2, \\ \gamma_2 \gamma_3 &= c_1 c_2 + g_1^2. \end{aligned}} \tag{186}$$

This proves Statement (ii)(b). □

E Proof of the Higher-Order Aircraft Limiting-Input Correspondence

Proof of Proposition 6 For the present design choice $H = \alpha_{\max} - \alpha$ and $\gamma_1^{\mathrm{HOCBF}} = \gamma_1^{\mathrm{OLB}}$, the first HOCBF quantity and the first OLB tracking error coincide, $\psi_1 = e_1$, according to Proposition 4.

Furthermore, under the gain relations in Eq. (102), Proposition 5 implies identical active dynamics of e_1 for HOCBF and OLB.

For the linear phase-plane boundary used here,

$$e_1 = \gamma_1^{\mathrm{OLB}}(\alpha_{\max} - \alpha) - \dot{\alpha},$$

and therefore

$$\ddot{e}_1 = -\gamma_1^{\mathrm{OLB}} \ddot{\alpha} - \alpha^{(3)}. \tag{187}$$

Hence, identical active e_1 dynamics require the same value of $\alpha^{(3)}$.

From Eq. (87), the difference between the values of $\alpha^{(3)}$ generated by the two limiting inputs is

$$0 = \frac{(1 + Z_q) M_\eta}{\tau_\eta} \left(\eta_{\mathrm{cmd,lim}}^{\mathrm{HOCBF}} - \eta_{\mathrm{cmd,lim}}^{\mathrm{OLB}} \right). \tag{188}$$

Since $(1 + Z_q) M_\eta \neq 0$ and $\tau_\eta > 0$, it follows that

$$\boxed{\eta_{\mathrm{cmd,lim}}^{\mathrm{HOCBF}} = \eta_{\mathrm{cmd,lim}}^{\mathrm{OLB}}}.$$

This proves the proposition. □

Declarations

Some journals require declarations to be submitted in a standardised format. Please check the Instructions for Authors of the journal to which you are submitting to see if you need to complete this section. If yes, your manuscript must contain the following sections under the heading 'Declarations':

- Funding

- Conflict of interest/Competing interests (check journal-specific guidelines for which heading to use)
- Ethics approval and consent to participate
- Consent for publication
- Data availability
- Materials availability
- Code availability
- Author contribution

If any of the sections are not relevant to your manuscript, please include the heading and write 'Not applicable' for that section.

References

Ahmad HMS, Sabouni E, Xiao W, et al (2025) Safe and secure control of connected and automated vehicles: An event-triggered control approach using trust-aware robust control barrier functions. ACM Transactions on Cyber-Physical Systems https://doi.org/10.1145/3776545

Altunkaya E, Çatak A, Demir M, et al (2026) Aircraft stability and safety: Practical applications of control lyapunov and barrier functions. Journal of Guidance, Control, and Dynamics 49(3):836–851. https://doi.org/10.2514/1.G008886

Ames AD, Grizzle JW, Tabuada P (2014) Control barrier function based quadratic programs with application to adaptive cruise control. In: Proceedings of the 53rd IEEE Conference on Decision and Control. IEEE, pp 6271–6278, https://doi.org/10.1109/CDC.2014.7040372

Ames AD, Xu X, Grizzle JW, et al (2017a) Control barrier function based quadratic programs for safety critical systems. IEEE Transactions on Automatic Control 62(8):3861–3876. https://doi.org/10.1109/TAC.2016.2638961

Ames AD, Xu X, Grizzle JW, et al (2017b) Control barrier function based quadratic programs for safety critical systems. IEEE Transactions on Automatic Control 62(8):3861–3876. https://doi.org/10.1109/TAC.2016.2638961

Autenrieb J (2025) Quadratic programming approach to flight envelope protection using control barrier functions. Journal of Guidance, Control, and Dynamics 48(11):2622–2633. https://doi.org/10.2514/1.G009203

Autenrieb J, Spiller M, Fisher PA, et al (2026) Closed-loop model-based control barrier functions with application to robust flight envelope protection. https://doi.org/10.48550/arXiv.2607.28830, arXiv:2607.28830

Bhatia P, Basu Roy S, Sujit PB, et al (2026) Decentralized nested control barrier functions for simultaneous formation control, collision avoidance, and connectivity maintenance. Journal of the Franklin Institute 363(12):108824. https://doi.org/10.

1016/j.jfranklin.2026.108824

Braun D, Steffensen R, Steinert A, et al (2022) Counter optimization-based testing of flight envelope protections in a fly-by-wire control law using deep q-learning. In: Proceedings of the 2022 CEAS EuroGNC Conference, Berlin, Germany, cEAS-GNC-2022-076

Feng S, de Castro R, Ebrahimi I (2024) Safe battery control using cascade-control-barrier functions. IEEE Transactions on Control Systems Technology 32(6):2344–2358. https://doi.org/10.1109/TCST.2024.3430708

Gabrys AC, Steffensen R, de Angelis Cordeiro R, et al (2019) Integration of phase plane flight envelope protections in cascaded incremental flight control. IFAC-PapersOnLine 52(12):429–435. https://doi.org/10.1016/j.ifacol.2019.11.281

Govoni L, Cristofaro A (2024) Decentralized task allocation for redundant multi-robot systems: An iterative consensus approach. In: 2024 IEEE 18th International Conference on Control & Automation (ICCA), pp 804–809, https://doi.org/10.1109/ICCA62789.2024.10591823

Gutierrez R, Hoagg JB (2025) Control barrier functions with real-time gaussian process modeling. URL https://arxiv.org/abs/2505.06765, arXiv:2505.06765

Hafner S, Autenrieb J, Steinert A, et al (2026) Control barrier functions on a pseudo control level for safe flight control. In: Proceedings of the 2026 CEAS EuroGNC Conference, Madrid, Spain, https://doi.org/10.82124/CEAS-GNC-2026-010

Heshmati-Alamdari S, Sharifi M, Karras GC, et al (2024) Control barrier function based visual servoing for mobile manipulator systems under functional limitations. Robotics and Autonomous Systems 182:104813. https://doi.org/10.1016/j.robot.2024.104813

Hsu KC, Hu H, Fisac JF (2024) The safety filter: A unified view of safety-critical control in autonomous systems. Annual Review of Control, Robotics, and Autonomous Systems 7:47–72. https://doi.org/10.1146/annurev-control-071723-102940

Karlsson E, Gabrys A, Schatz SP, et al (2016) Dynamic flight path control coupling for energy and maneuvering integrity. In: 2016 14th International Conference on Control, Automation, Robotics and Vision (ICARCV). IEEE, pp 1–6, https://doi.org/10.1109/ICARCV.2016.7838678

Li Z, Atanasov N (2023) Governor-parameterized barrier function for safe output tracking with locally sensed constraints. Automatica 152:110996. https://doi.org/10.1016/j.automatica.2023.110996

Liang K, Cai M, Vasile CI (2024) Control barrier function for linearizable systems with high relative degrees from signal temporal logics: A reference governor approach. In:

2024 American Control Conference (ACC), https://doi.org/10.23919/ACC60939.2024.10644886

Liu B, Rocco P, Zanchettin AM, et al (2024) A real-time hierarchical control method for safe human–robot coexistence. Robotics and Computer-Integrated Manufacturing 86:102666. https://doi.org/10.1016/j.rcim.2023.102666

Maithani P, Arab A, Khorrami F, et al (2026) Proactive hierarchical control barrier function-based constraint prioritization to enhance safety in human–robot interaction. Control Engineering Practice 166:106624. https://doi.org/10.1016/j.conengprac.2025.106624

Nguyen Q, Sreenath K (2016) Exponential control barrier functions for enforcing high relative-degree safety-critical constraints. In: Proceedings of the American Control Conference (ACC). IEEE, pp 322–328, https://doi.org/10.1109/ACC.2016.7524935

Prajna S, Jadbabaie A (2004) Safety verification of hybrid systems using barrier certificates. In: Hybrid Systems: Computation and Control, Lecture Notes in Computer Science, vol 2993. Springer, pp 477–492, https://doi.org/10.1007/978-3-540-24743-2_32

Qin L, Yang T, Lang J (2026) Towards transient frequency safety: A novel load frequency control with wind-storage system via control barrier function. Journal of Energy Storage 153:120975. https://doi.org/10.1016/j.est.2026.120975

Rabiee P, Hoagg JB (2025) Soft-minimum and soft-maximum barrier functions for safety with actuation constraints. Automatica 171:111921. https://doi.org/10.1016/j.automatica.2024.111921

Sabouni E, Cassandras CG, Xiao W, et al (2024) Optimal control of connected automated vehicles with event/self-triggered control barrier functions. Automatica 162:111530. https://doi.org/10.1016/j.automatica.2024.111530

Schneeberger M, Dörfler F, Mastellone S (2024) Advanced safety filter for smooth transient operation of a battery energy storage system. In: Proceedings of the IEEE Conference on Decision and Control, pp 2385–2390, https://doi.org/10.1109/CDC56724.2024.10886256

Sharma VK, Zhou P, Xu Z, et al (2025) Safe human–robot collaboration with risk tunable control barrier functions. IEEE/ASME Transactions on Mechatronics 30(4):3133–3141. https://doi.org/10.1109/TMECH.2025.3572047

Steffensen R, Gabrys A, Holzapfel F (2019a) Flight envelope protections using phase plane limits and backstepping control. In: Proceedings of the 2019 CEAS EuroGNC Conference, Milan, Italy, cEAS-GNC-2019-003

Steffensen R, Gabrys A, Holzapfel F (2019b) Flight envelope protections using phase plane limits and backstepping control. In: Proceedings of the 2019 CEAS EuroGNC Conference, Milan, Italy, cEAS-GNC-2019-003

Steffensen R, Steinert AC, Holzapfel F (2022) Longitudinal incremental reference model for fly-by-wire control law using incremental non-linear dynamic inversion. In: AIAA SciTech Forum. American Institute of Aeronautics and Astronautics, https://doi.org/10.2514/6.2022-1230

Tan X, Dimarogonas DV (2024) On the undesired equilibria induced by control barrier function based quadratic programs. Automatica 159:111359. https://doi.org/10.1016/j.automatica.2023.111359

Vinter-Hviid F, Sloth C, Savarimuthu TR, et al (2024) Safe contact-based robot active search using bayesian optimization and control barrier functions. Frontiers in Robotics and AI 11:1344367. https://doi.org/10.3389/frobt.2024.1344367

Wang H, Peng J, Zhang F, et al (2024) High-order control barrier function-based safety control of constrained robotic systems: An augmented dynamics approach. IEEE/-CAA Journal of Automatica Sinica 11(12):2487–2496. https://doi.org/10.1109/JAS.2024.124524

Wang Y, Ji Z, Zhou C, et al (2025) Control barrier function based dynamic flexibility analysis in infinite time domain for industrial processes. Chemical Engineering Research and Design 216:90–105. https://doi.org/10.1016/j.cherd.2025.02.019

Wieland P, Allgöwer F (2007) Constructive safety using control barrier functions. IFAC Proceedings Volumes 40(12):462–467. https://doi.org/10.3182/20070822-3-ZA-2920.00076

Xiao W, Belta C (2019) Control barrier functions for systems with high relative degree. In: 2019 IEEE 58th Conference on Decision and Control (CDC), pp 474–479

Xiao W, Belta C (2022) High-order control barrier functions. IEEE Transactions on Automatic Control 67(7):3655–3662. https://doi.org/10.1109/TAC.2021.3105491

Xiong Y, Zhai DH, Zhang S, et al (2026) Enhancing safety in uncertain robotic systems via control barrier functions and PD control. International Journal of Robust and Nonlinear Control 36(6):3354–3365. https://doi.org/10.1002/rnc.70347

Zhang F, Holzapfel F (2015) Flight control using physical dynamic inversion. In: AIAA Guidance, Navigation, and Control Conference. American Institute of Aeronautics and Astronautics, https://doi.org/10.2514/6.2015-1758

Zhang F, Holzapfel F, Heller M (2013) Nonlinear non-cascaded reference model architecture for flight control design. Springer, https://doi.org/10.1007/978-3-642-38253-6_25

Zhang F, Braun S, Holzapfel F (2014) Physically integrated reference model and its aids in validation of requirements to flight control systems. In: AIAA Guidance, Navigation, and Control Conference. American Institute of Aeronautics and Astronautics, https://doi.org/10.2514/6.2014-0962